ORIGINAL ARTICLE

Generalized eddy–diffusivity mass–flux (GEM) formulation for the parameterization of atmospheric convection and turbulence

Cristian V. Vraciu[1,2]

[1]Faculty of Physics, University of Bucharest, Bucharest–Măgurele, Romania

[2]Department of Theoretical Physics, Horia Hulubei National Institute of Physics and Nuclear Engineering, Măgurele, Romania

Correspondence
Cristian V. Vraciu, Faculty of Physics, University of Bucharest, Bucharest–Măgurele, RO–077125, Romania
Email: cristian.vraciu@s.unibuc.ro

Funding information
Romanian Ministry of Research, Innovation and Digitisation, Grant/Award Number: PN 23 21 01 01

The atmospheric convection is a phenomenon that has a length scale smaller than the resolution at which the state–of–the–art general circulation numerical models are running, and thus, the convection needs to be parameterized. In this work, a theoretical formulation for the parameterization of subgrid–scale convection based on subgrid averaging that represents a generalized eddy–diffusivity mass–flux (GEM) formulation is presented. The subgrid fluxes are derived by considering a decomposition of subgrid variables into convective and turbulent variables, and by assuming that the convection is modeled by round convective plumes with generic radial profiles. The main difference between our formulation and the mass–flux formulations is that the condition of a very small fractional area occupied by the convection is replaced with the condition that the convective vertical velocity goes to the mean state far from the updraft region of the plume. The plume model can be also generalized by considering that the convective elements are energy–consistent plumes, governed by the conservation of mass, momentum, kinetic energy, and buoyancy, which provides a physical–based closure for the entrainment. Therefore, the closing problem of our formulation consists of the specification of the convective radial profiles and the boundary conditions at the initial vertical

level. Furthermore, our formulation allows one to consider more realistic profiles for the convective variables, making the formulation suitable for the parameterization of atmospheric convection at the convective gray–zone. This aspect is discussed in the last part of this work, where it is showed how the formulation can be implemented at any resolution. Moreover, in the present framework, no distinct assumptions are required for each convective type, thus facilitating the parameterization of convection in a unified way.

KEYWORDS
atmospheric convection, unified parameterization, gray–zone, plume model, turbulence

1 | INTRODUCTION

The majority of the modern numerical models use parameterization schemes for the representation of the moist convection based on the so-called mass–flux formulation, in which it is assumed that the convective elements (such as cumulus clouds and dry updrafts) are steady–state convective plumes. The representation of convection is typically split into separate parameterization schemes for dry, shallow, and deep convection, respectively, and all are based on different theoretical considerations. Unfortunately, little progress has been made for improving the physical basis of the parameterization of deep convection since Arakawa and Schubert (1974), Tiedtke (1989) and Kain and Fritsch (1990). For this reason, the representation of deep convection is still a large source of error in weather and climate prediction models (Holloway et al., 2014; Yin and Porporato, 2017; Sherwood et al., 2020; Masson-Delmotte et al., 2021). The traditional parameterizations heavily rely on the assumption of quasi–equilibrium and a very small fractional area occupied by the convection, which requires a very large grid spacing of the numerical models. Due to the increasing computational power, the general circulation models run nowadays at a resolution at which the quasi–equilibrium assumption does not hold. Therefore, for this reason, some parameterization schemes with relaxed quasi–equilibrium condition have been developed (e.g. Pan and Randall, 1998; Gerard and Geleyn, 2005; Park, 2014).

At the same time, stochastic parameterizations for deep (e.g. Plant and Craig, 2008; Hagos et al., 2018; Bengtsson et al., 2022) and shallow convection (e.g. Sakradzija et al., 2016; Sakradzija and Klocke, 2018; Shin and Park, 2020) have been proposed in order to make the mass–flux formulation more suitable for numerical simulation at the convective gray–zone. However, the assumption of a very small fractional area occupied by the convection in every grid–box of the numerical model is still a very important assumption in all mass–flux formations (Yano, 2014b; Arakawa and Wu, 2015), which means that the grid spacing of the numerical models must be large enough such that this condition is respected regardless of the spatial variability of the convective elements. Although parameterizations with relaxed fractional area occupied by the convection have been formulated (e.g. Arakawa and Wu, 2013; Grell and Freitas, 2014; Fan et al., 2015; Gerard, 2015; Zheng et al., 2016; Kwon and Hong, 2017; Malardel and Bechtold, 2019; Langguth et al., 2020; Wang, 2022), they still assume top–hat profiles as in the mass–flux formulation, and as is going to be seen in Section 4.3.1, such development is valid only if the convective radial velocity is assumed to be very small, and thus, the

subgrid fluxes containing subgrid horizontal wind components, such as the subgrid horizontal transport, are neglected. However, at high resolutions, there might be a large variability between two consecutive grid cells (for example, in a grid cell a cumulonimbus cloud may develop, while in the neighbor one only shallow convection is present), and thus, neglecting the subgrid horizontal transport terms might result in large errors. Furthermore, although these schemes relax the condition of a small fractional area occupied by the convection in the subgrid vertical transport term, this condition is usually still present in the plume model they assume since it is considered that the plume entrains environmental air in which the environmental variables are still assumed to be equal with the mean grid–box variables. Under the present development, this inconsistency is also avoided. Moreover, in the schemes with relaxed fractional area occupied by the convection, which considers top–hat profiles for the convective elements, it is assumed that the convection is fully resolved when the horizontal resolution is equal to the horizontal dimension of a cloud, which is on the order of 1 km, although in fact a resolution of ~ 100 m is required to adequately resolve the convective clouds and the mesoscale organization of the cloud ensemble (Bryan et al., 2003; Lebo and Morrison, 2015; Jeevanjee, 2017; Savre and Craig, 2023). More recently, in order to circumvent many of the problems associated with the mass–flux parameterization at the gray–zone, an alternative framework based on conditional filtering has been developed by Thuburn et al. (2018). A similar framework that generalizes the mass–flux formulation has been previously proposed by Yano et al. (2010) or Yano (2012, 2016), in which the flow is decomposed in a number of components that are assumed to be constant within a grid cell.

Due to their proven practicality in a wide range of domains, machine–learning algorithms have been also recently proposed as a solution to improve the parameterization of atmospheric convection (e.g. O'Gorman and Dwyer, 2018; Yuval and O'Gorman, 2020; Hagos et al., 2022; Kriegmair et al., 2022; Lopez-Gomez et al., 2022; Shin and Baik, 2022), but their practical usage and implementation is not very clear yet and this research topic is still in an incipient stage. Since these algorithms only adjust some coefficients depending on the large-scale conditions, it might be beneficial to make sure that they build on physical–based models in order to ensure that the conservation laws are reasonably respected.

As in the mass–flux formulation, in this work we develop a theoretical formulation for the parameterization of the subgrid–scale convection following the grid–box averaging technique, obtaining a generalized eddy–diffusivity mass–flux (GEM) formulation. However, the main difference between our formulation and the mass–flux scheme is that we do not assume the subgrid to consist of top–hat plumes with a very small fractional area and an environment that occupies the rest of the subgrid, both treated independently as two separated fluids that can interact with each other through lateral entrainment and detrainment. We rather assume that the convective variables are described by a plume located in the center of their system which gradually transitions into an environmental state at infinity. In this way, we provide a more general treatment in which the convective fluxes can be obtained without assuming that the fractional area occupied by the convection is very small as in the mass–flux formulation. It is shown, however, that if one assumes top–hat profiles, then our assumptions become equivalent to the mass–flux ones since a plume with a top–hat will transition to the environmental state at infinity only if the fractional area occupied by the convection is very small. Nonetheless, for realistic radial profiles, the assumption of a very small fractional area occupied by the convection becomes relaxed, thus making our formulation more suitable for simulations at the convective gray–zone. Following the seminal work of Priestley and Ball (1955), we also consider an energy–consistent plume model, which means that we introduce, in addition, an equation for the vertical component of the kinetic energy. By doing so, we generalize the classical entraining plume model and provide a physical–based closure for the entrainment, whose parameterization problem is notorious for being the principal source of errors in the representation of the subgrid–scale convection (Murphy et al., 2004; Klocke et al., 2011). The energy–consistent plume model has been proven by both numerical simulations and experimental studies to predict with a high accuracy the convective flow of plumes

in idealised setups (e.g. Wang and Law, 2002; Kaminski et al., 2005; Ezzamel et al., 2015; van Reeuwijk and Craske, 2015; van Reeuwijk et al., 2016; Kewalramani et al., 2022; Milton-McGurk et al., 2023). Therefore, as also suggested by Savre and Herzog (2019), Vraciu (2022) or Yano (2023), we believe that the energy–consistent plume model can also be a better choice for modeling the atmospheric subgrid–scale convection than the entraining plume model that is currently used in the mass–flux formulations. Although the energy–consistent plume model requires closure for the radial profiles of the convective plume, switching the closure problem from entrainment to radial profiles, it has the advantage of providing a physical–based entrainment and of allowing to consider more realistic radial profiles for the plume model. Therefore, as it is going to be seen, the whole parameterization problem only reduces to the specification of certain radial coefficients. However, considering the energy–consistent plume model is not crucial for the present formulation, since the classical entraining plume model can be recovered from the more generic energy–consistent plume model.

Another potential advantage of the energy–consistent plume model is that does not require distinct theoretical considerations for every convective type, and thus, dry, shallow, and deep convection can all be parameterized in a unified way, which eliminates the necessity of triggering functions. This unified treatment has been already proposed by building on the traditional mass–flux formulation (e.g. Hohenegger and Bretherton, 2011; D'Andrea et al., 2014), while others formulated unified parameterization schemes following the eddy–diffusivity mass–flux approach (e.g. Rio et al., 2009; Angevine et al., 2010; de Roode et al., 2012; Sušelj et al., 2012; Sakradzija et al., 2016; Han and Bretherton, 2019; Suselj et al., 2019; Cohen et al., 2020; Witte et al., 2022; Suselj et al., 2022; Smalley et al., 2022). In the unified schemes, the convective plumes are initialized at the first vertical level in the surface layer, and are allowed to rise and condense at the lifting condensation level forming cumulus clouds. Above the condensation level, depending on the large scale stability condition, the plumes will either develop into cumulonimbus clouds or will remain shallow. However, different types of entrainment closures are assumed and different values for the plumes radii are considered depending on their type, and thus, the plumes are not represented completely in a unified way. As it is going to be seen in Section 4, the energy–consistent plume model does not require closure for the entrainment and provides an equation for the plume radius. Therefore, the energy–consistent plume model could be a more suitable choice for the representation of atmospheric convection in a unified way. In addition, approximate analytical solutions for the proposed plume model are obtained, facilitating the implementation of the plume model in numerical models with a high vertical grid spacing. Furthermore, in the last part of this work, it is shown how the present formulation can be implemented in a high–resolution numerical model at the convective gray–zone.

Moreover, in this work, we derive the expressions for the subgrid fluxes for generic radial profiles and we discuss the situation in which every convective plume is characterised by an updraft located in the center and a subsidising shell around the updraft area, as it follows from the recent observational and numerical evidence (Mallaun et al., 2019; Griewank et al., 2020; Nair et al., 2020; Gu et al., 2021; Savre, 2021; Denby et al., 2022). We show that for such a profile of the convective vertical velocity we can obtain the subgrid fluxes without requiring that the fractional area occupied by the convection in a given grid box be very small. Furthermore, it is discussed in Section 7 how the present formulation can be implemented for simulations with resolutions for which the fractional area occupied by the convection is close to 1, and it is shown that even in this limit the convection remains partially parameterized if proper radial profiles are considered. Under this case, the convection becomes fully resolved only at resolutions much smaller than the horizontal dimension of the convective plumes.

2 | MASS–FLUX FORMULATION

2.1 | Traditional mass–flux scheme

As already discussed, the majority of the current parameterization models for deep and shallow convection are the so–called mass–flux parameterizations. In these schemes, it is assumed that the total subgrid flux of a variable φ is represented by the subgrid vertical flux $\overline{\varphi^* w^*}$ (Arakawa and Schubert, 1974; Plant and Yano, 2016) given by:

$$\rho\overline{\varphi^* w^*} = M(\varphi_c - \overline{\varphi}), \tag{1}$$

where $M = \rho\sigma w_c'$ is the convective mass flux, ρ is the atmospheric density, σ is the fractional area occupied by the convective plume, w_c' is the characteristic vertical velocity of the plume, and φ_c and $\overline{\varphi}$ are the convective and mean values of the variable φ, respectively. In the traditional mass–flux formulation $\sigma \ll 1$ is considered, making no difference between the environmental and the mean variables.

The dynamics of the subgrid–scale convection are described by steady–state axisymmetric plumes. For every convective plume, the governing equation for the convective variables φ_c is given by (Arakawa and Schubert, 1974):

$$\frac{\partial}{\partial z} M\varphi_c = E\overline{\varphi} - D\varphi_c + \sigma F', \tag{2}$$

where z is the vertical coordinate, E is the entrainment rate, D is the detrainment rate and F' is the convective–scale forcing on φ_c. Note that this equation is only valid in the limit $\sigma \ll 1$ because the plume entrains environmental air in which the environmental variable is assumed equal to the mean variable $\overline{\varphi}$. At the gray–zone, this condition must also be relaxed. Also, the mass flux M is usually separated into a normalized vertical dependent profile $\mu(z)$ and a temporal dependent amplitude $M_B(t)$ defined at the cloud base:

$$M(z,t) = \mu(z)\ M_B(t). \tag{3}$$

The problem of defining μ and M_B are called "cloud model" and "closure", respectively. Review articles such as Plant (2010) or Yano et al. (2013) discuss the closure problem, in which the objective is to find a relation for the mass flux amplitude M_B as a function of the atmospheric instability. On the other hand, in the traditional mass–flux parameterizations, the cloud model problem is closed using the Morton et al. (1956) entrainment hypothesis (Arakawa and Schubert, 1974; Plant, 2010; Yano, 2014a). Recall that the entrainment hypothesis states that the horizontal inflow in the convective plume is proportional to the characteristic vertical velocity of the plume (Turner, 1986):

$$-(ru_r')_{r=R} = \alpha_e R w_c', \tag{4}$$

where r is the radial coordinate in the cylindrical system, u_r' is the radial velocity of the plume, R is the plume radius, and α_e is a constant, known as the entrainment coefficient. Thus, using the entrainment hypothesis, the continuity equation reduces to:

$$\frac{d}{dz}(w_c' R^2) = \alpha_e R w_c'. \tag{5}$$

Since $\sigma \propto R^2/A$, in which A is the grid–box area, the continuity equation becomes:

$$\frac{1}{\mu}\frac{d}{dz}\mu = \frac{\alpha_e}{R}. \tag{6}$$

In addition, in the mass–flux formulations, the plume radius R is assumed to be constant in the Lagrangian sense (de Rooy et al., 2013; Plant and Yano, 2016), which leads to the following normalized profile:

$$\mu = \exp\left[\frac{\alpha_e}{R}(z - z_B)\right], \tag{7}$$

where z_B is the cloud base height. Following the entrainment hypothesis, the fractional entrainment rate $\epsilon = E/M$ is given by: $\epsilon = \alpha_e/R$.

Therefore, one can see that in the traditional mass-flux formulations, the atmospheric instability only controls the mass flux amplitude but not its profile, which is only controlled by the turbulent entrainment, since the entrainment hypothesis only takes into consideration the turbulent entrainment for a self–similar flow (Bejan, 2013; van Reeuwijk and Craske, 2015). In addition, the plume radius is usually assumed constant (Arakawa and Schubert, 1974; Plant, 2010; Yano et al., 2013; Yano, 2014b; de Rooy et al., 2013), which is inconsistent with the Morton et al. (1956) model, since the entrainment hypothesis is based on the observation that the convective plume radius is proportional with z (Bejan, 2013). Of course, over the years, numerous large eddy simulations (LES) of deep convection showed that in reality, the mass flux does not follow the exponential profile given by relation (7) (e.g. Khairoutdinov et al., 2009; Romps and Charn, 2015; Peters et al., 2021). Moreover, the plume is assumed to detrain instantaneously at the level of neutral buoyancy, which is also an unphysical behavior as proven by numerous LES simulations (e.g. Romps, 2010; Dawe and Austin, 2011; Peters et al., 2020). In order to improve the mass–flux formulation, many other entrainment parameterizations have been proposed. For example, Gregory (2001) assumes $\epsilon \propto B_c'/w_c'^2$ and von Salzen and McFarlane (2002) assumes $\epsilon \propto dB_c'/dz$, where B_c' is the plume buoyancy. Neggers et al. (2002) considers $\epsilon = 1/(\tau w_c')$, where τ is a constant cloud lifetime, assumed to follow a stochastic variability by Sakradzija et al. (2016). The reader is referred to the paper of de Rooy et al. (2013) for a comprehensive review of the assumed entrainment parameterization in the cumulus convection.

At the same time, in order to better represent the vertical structure of shallow and deep convection, parameterization schemes that use in addition an equation for the plume updraft velocity of the form

$$\frac{1}{2}\frac{\partial w_c'^2}{\partial z} = \mathrm{a}B_c' + \mathrm{b}\epsilon w_c'^2 \tag{8}$$

have been developed (e.g. Bechtold et al., 2001; Bretherton et al., 2004; Hohenegger and Bretherton, 2011; Kim and Kang, 2012; Chu and Lin, 2023), in which a and b are coefficients that requires closure.

2.2 | Eddy–diffusivity mass–flux scheme

The eddy–diffusivity mass–flux (EDMF) parameterization combines the effects of turbulent eddies that are modeled using the eddy–diffusivity model and the effect of convective updrafts on the large–scale variables (Hourdin et al., 2002; Soares et al., 2004). Thus, the subgrid vertical flux is given by:

$$\overline{\rho\varphi^* w^*} = M(\varphi_c - \overline{\varphi}) + \rho K_\varphi \frac{\partial \overline{\varphi}}{\partial z}, \tag{9}$$

where K_φ is the eddy diffusivity of the scalar φ. The eddy diffusivity term from Equation 9 represents the turbulent mixing only in the environment, and thus, the condition $\sigma \ll 1$ should be considered. However, as is going to be seen, such an assumption is not necessarily required under the present formulation.

The EDMF has been initially proposed for the parameterization of the dry boundary layer, in which the dry updrafts are assumed to be round convective plumes. In the EDMF parameterization, the dry plumes are modeled using an equation for the plume updraft velocity given by Equation 8, and for the conserved convective variables φ_c:

$$\frac{d\varphi_c}{dz} = -\epsilon(\varphi_c - \overline{\varphi}). \tag{10}$$

The system of Equations 8 and 10 represents the one–dimensional Lagrangian plume model, also referred to as the entraining plume model.

In the standard procedure of the entraining plume model the fractional entrainment rate is closed using the entrainment hypothesis as in the traditional mass–flux formulation (Houze, 2014). However, in the EDMF formulations, many other entrainment parameterizations have been assumed. For example, based on LES results, de Roode et al. (2000) proposed that:

$$\varepsilon \propto z^{-\beta}, \tag{11}$$

where β is a constant with a value close to 1. Siebesma and Teixeira (2000), Soares et al. (2004) and Siebesma et al. (2007), based on LES and empirical evidence, consider that the fractional entrainment is given by:

$$\varepsilon \propto \left(\frac{1}{z} + \frac{1}{z_i - z}\right), \tag{12}$$

where z_i is the inversion height of the dry boundary layer. On the other hand, Pergaud et al. (2009) consider as in Gregory (2001) that $\epsilon \propto B_c'/w'^2$ based on scaling arguments. Vraciu (2022) showed that by following the Priestley and Ball (1955) formalism one may obtain the system of Equations 8 and 10 with a fractional entrainment rate that scales as $\epsilon \propto z^{-1}$ in which the plume radius is not assumed constant but follows a linear growth with the height, giving thus a theoretical explanation for the entrainment parameterization closures assumed by de Roode et al. (2000), Siebesma and Teixeira (2000), Soares et al. (2004) and Siebesma et al. (2007).

An extended version of the EDMF formulation has been proposed by Tan et al. (2018) in which prognostic plumes are assumed to model the updrafts and downdrafts, and it is considered that the second–order moments can be

partitioned between the plumes and the environment, which could be more suitable for the convective gray–zone.

It might deserve mentioning that the EDMF parameterization has been criticized by some authors because it combines the mass–flux formulation and the eddy–diffusivity parameterization without any regard for mutual consistency, which may lead to physical inconsistencies (Yano et al., 2016, 2018). These authors argue that rather than trying to put together schemes that have been developed independently, a better strategy would be to construct a unified scheme from scratch. This is exactly the procedure we adopt in this work, where a unified subgrid–scale parameterization is constructed by starting from the conservation laws and considering certain approximations. Furthermore, as it is going to be seen, the EDMF parameterization can be recovered from our formulation, which may show that the EDMF schemes are in fact physically consistent.

3 | STATEMENT OF THE PROBLEM

The convection parameterization problem can be considered as consisting of two parts: (1) the control of the large–scale (grid–scale) dynamics over the convection, which needs to be described by convective–scale (subgrid–scale) equations, and (2) the feedback provided by convection on the large–scale variables, which must be described by proper convective source terms on the large–scale equations. Thus, the objective of a parameterization theory is to obtain a closed set of equations for the large–scale and convective–scale variables, respectively.

We consider that the grid–point value of an atmospheric model represents a grid–box mean value. Thus, by taking an average over a grid box, the prognostic equations for the mean variables in Cartesian coordinates, considering the Einstein notation, in the anelastic approximation, are given by:

$$\frac{\partial}{\partial t}(\overline{w}) + \frac{1}{\rho}\frac{\partial}{\partial z}(\rho\overline{w}^2) + \frac{\partial}{\partial x_j}(\overline{w}\,\overline{u_j}) = Q_w, \tag{13}$$

$$\frac{\partial}{\partial t}(\overline{u_i}) + \frac{1}{\rho}\frac{\partial}{\partial z}(\rho\overline{u_i}\,\overline{w}) + \frac{\partial}{\partial x_j}(\overline{u_i}\,\overline{u_j}) = Q_{u_i}, \tag{14}$$

$$\frac{\partial}{\partial t}(\overline{\varphi}) + \frac{1}{\rho}\frac{\partial}{\partial z}(\rho\overline{w}\,\overline{\varphi}) + \frac{\partial}{\partial x_j}(\overline{\varphi}\,\overline{u_j}) = Q_\varphi, \tag{15}$$

where t is the time coordinate, ρ is the atmospheric density which is only a function of z (the anelastic approximation), $\overline{u_i}$ is the mean horizontal wind in the x_i direction, with $i, j = \overline{1,2}$, $\overline{w}$ is the mean vertical velocity in the z direction, with z taken along the mean gravitational acceleration, $\overline{\varphi}$ is the mean value of the scalar φ, which represents any scalar other than the components of the flow, and Q_w, Q_{u_i} and Q_φ represent the apparent source terms for $\overline{w}$, $\overline{u_i}$ and $\overline{\varphi}$, respectively. The apparent source terms are given by:

$$Q_w = -\frac{1}{\rho}\frac{\partial}{\partial z}(\rho\overline{w^{*2}}) - \frac{\partial}{\partial x_j}\overline{(w^* u_j^*)} + \overline{F_w}, \tag{16}$$

$$Q_{u_i} = -\frac{1}{\rho}\frac{\partial}{\partial z}(\rho\overline{u_i^* w^*}) - \frac{\partial}{\partial x_j}\overline{(u_i^* u_j^*)} + \overline{F_{u_i}}, \tag{17}$$

$$Q_{\varphi} = -\frac{1}{\rho}\frac{\partial}{\partial z}(\rho\overline{\varphi^* w^*}) - \frac{\partial}{\partial x_j}\overline{(\varphi^* u_j^*)} + \overline{F_{\varphi}}, \tag{18}$$

where w^* is the subgrid vertical velocity, u_i^* is the subgrid horizontal velocity in the x_i direction, φ^* is the subgrid scalar, and $\overline{F_w}$, $\overline{F_{u_i}}$ and $\overline{F_{\varphi}}$ are the large–scale and other forcings for $\overline{w}$, $\overline{u_i}$ and $\overline{\varphi}$, respectively. The form of the apparent source terms is obtained by considering that the starred variables are a deviation from the grid–box mean (e.g., $\varphi^* = \varphi - \overline{\varphi}$), which means that $\overline{w^*} = \overline{u_i^*} = \overline{\varphi^*} = 0$. The box has a size of $L_{x1} \times L_{x2}$ in the x_1 and x_2 directions, respectively. The grid–box averaging operator $\overline{(\cdot)}$ is given by:

$$\overline{(\cdot)} = \frac{1}{L_{x1}L_{x2}}\int_{-L_{x1}/2}^{+L_{x2}/2}\int_{-L_{x2}/2}^{+L_{x2}/2} dx_1 dx_2. \tag{19}$$

The first two terms of the apparent source terms represent the subgrid fluxes, which provide the feedback of the convection and turbulence upon the large–scale variables. The objective of any subgrid–scale convective parameterization is to find appropriate expressions for these fluxes.

As shown by Pinsky et al. (2021), we can decompose the subgrid variables into convective and turbulent components, say $w^* = w' + w''$, where we denote with prime the convective variables and with double prime the turbulent ones. Since $\overline{w^*} = 0$, as imposed before, and by definition $\overline{w''} = 0$, it requires that $\overline{w'} = 0$. Thus, since we consider the grid–box averaging on the horizontal plane, the horizontal profile of the convective variables must be chosen in such a way that the condition $\overline{w^*} = 0$ is respected at every height and time (similar for φ^* and u_i^*).

4 | THE PLUME MODEL

We assume that the convective motion is characterized by steady–state round convective plumes, in such a way that the condition $\overline{w'} = \overline{\varphi'} = 0$ is respected. We also consider round plumes, and thus, we prefer to work in a cylindrical system of coordinates. For one plume, we consider that the governing equations are given by the continuity equation, the vertical momentum equation, the equation for the vertical component of the kinetic energy, and the advection–diffusion equations, in the anelastic approximation as:

$$\frac{\partial}{\partial z}(r\rho w') + \frac{\partial}{\partial r}(r\rho u_r') = 0, \tag{20}$$

$$\frac{\partial}{\partial z}(r\rho w'^2) + \frac{\partial}{\partial r}(r\rho u_r' w') = r\rho B' - \frac{\partial}{\partial r}(r\rho\tau_w), \tag{21}$$

$$\frac{\partial}{\partial z}\left(\frac{1}{2}r\rho w'^3\right)+\frac{\partial}{\partial r}\left(\frac{1}{2}r\rho u_r' w'^2\right)=r\rho w' B'-w'\frac{\partial}{\partial r}(r\rho\tau_w), \tag{22}$$

$$\frac{\partial}{\partial z}(r\rho w'\varphi')+\frac{\partial}{\partial r}\left(r\rho u_r'\varphi'\right)=-\frac{\partial}{\partial r}(r\rho\tau_\varphi)-r\rho w'\frac{\partial\overline{\varphi}}{\partial z}+r\rho F_\varphi', \tag{23}$$

where u_r' is the plume's radial velocity in the r direction, τ_w is the radial turbulent shearing stress, τ_φ is the radial turbulent diffusion flux of the scalar φ' and F_φ' is the convective source term of the scalar φ. The derivation of the system of governing Equations 20–23 is presented in Appendix A. Here, the kinetic–energy equation is introduced only for the generalization of the plume model, and as it is going to be seen, the classical entraining plume model can be easily recovered under the present formulation. The specification of the convective source terms depends on the chosen microphysics parameterization, which is beyond the scope of this work since we do not want to lose the generality of the formulation. We also neglect here the earth's rotation on the plume dynamics. Although Deremble (2016) suggests that this effect might be important for the dynamics of the convective plumes, it is still unclear if such an effect must be considered by the convective parameterization models. The buoyancy force B' is given by:

$$B'=\frac{g}{\theta_{v0}}\theta_v'-gq_h', \tag{24}$$

where g is the gravitational acceleration, θ_{v0} is the reference virtual potential temperature, θ_v' is the convective–scale virtual potential temperature and q_h' is the convective–scale hydrometer mixing ratio. Thus, for the buoyancy, we have the equation:

$$\frac{\partial}{\partial z}(r\rho w' B')+\frac{\partial}{\partial r}\left(r\rho u_r' B'\right)=-\frac{\partial}{\partial r}\left(r\rho\tau_B\right)-r\rho w' N^2, \tag{25}$$

where $\tau_B=(g/\theta_{v0})\tau_{\theta v}-g\tau_{qh}$ is the buoyancy radial turbulent diffusion flux, and where N^2 is the Brunt–Vaisala frequency, defined here as:

$$N^2=\frac{g}{\theta_{v0}}\frac{\overline{\theta_v}}{\partial z}+g\frac{\partial\overline{q_h}}{\partial z}-\frac{1}{w'}\left(\frac{g}{\theta_{v0}}F_{\theta v}'+gF_{qh}'\right), \tag{26}$$

in which $F_{\theta v}'$ and F_{qh}' are the cloud source terms for the convective–scale virtual temperature and hydrometer mixing radio, respectively.

We assume that the convective–scale variables follow self–similar radial profiles:

$$\begin{aligned} &w'=w_c' f_w\left(\frac{r}{R}\right),\quad \varphi'=\varphi_c' f_\varphi\left(\frac{r}{R}\right),\quad u_r'=u_c' f_u\left(\frac{r}{R}\right),\\ &\tau_w=w_c'^2 f_\tau\left(\frac{r}{R}\right),\quad \tau_\varphi=w_c'\varphi_c' j_\varphi\left(\frac{r}{R}\right), \end{aligned} \tag{27}$$

where w_c' is the centerline vertical velocity of the plume, φ_c' is the centerline scalar, u_c' is the characteristic radial velocity, and f_w, f_φ, f_u, f_τ and j_φ are the radial profiles for the vertical velocity, scalar φ, radial velocity, radial turbulent shearing stress and radial turbulent diffusion flux, respectively. The radial profiles are chosen in such a way that they follow the condition $\overline{w'} = \overline{\varphi'} = 0$. In Section 4.3 two possible closures for the radial profiles are discussed.

4.1 | Conservation equations

The momentum Equation 21, the kinetic energy Equation 22, and the scalar Equation 23 can be integrated over the plume domain (from 0 to R), where we define the plume radius R as the distance from the center of the plume to the first r at which $w' = 0$. Therefore, by the definition of R, $f_w(1) = 0$. Thus, integrating Equations 21 – 23 from 0 to R, we obtain:

$$\frac{1}{\rho}\frac{d}{dz}\left[a_1\rho w_c'^2 R^2\right] - w_c'^2 f_w^2(1) R\frac{dR}{dz} = a_2 B_c' R^2 - w_c'^2 R f_\tau(1), \tag{28}$$

$$\frac{1}{\rho}\frac{d}{dz}\left[\frac{1}{2}a_3\rho w_c'^3 R^2\right] - \frac{1}{2}\rho w_c'^3 f_w^3(1) R\frac{dR}{dz} = a_4 w_c' B_c' R^2 - a_5 R w_c'^3 \tag{29}$$

$$\frac{1}{\rho}\frac{d}{dz}\left[a_\varphi\rho\varphi_c' w_c' R^2\right] - \varphi_c' w_c' f_\varphi(1) f_w(1) R\frac{dR}{dz} = -a_6 w_c' R^2\frac{\partial\overline{\varphi}}{\partial z} - R w_c'\varphi_c' j_\varphi(1) + J_c^\varphi, \tag{30}$$

where we used the Leibniz integral rule to perform the integrals over d/dz. $J_c^\varphi = \int_0^R F_\varphi' r\,dr$ is the integral convective source term, and the coefficients a_1 – a_6 and a_φ are given by:

$$\begin{aligned}
a_1 &= \int_0^1 f_w^2(\xi)\xi d\xi, \quad a_2 = \int_0^1 f_B(\xi)\xi d\xi, \quad a_3 = \int_0^1 f_w^3(\xi)\xi d\xi,\\
a_4 &= \int_0^1 f_w(\xi) f_B(\xi)\xi d\xi, \quad a_5 = \int_0^1 \frac{df_w(\xi)}{d\xi} f_\tau(\xi)\xi d\xi,\\
a_\varphi &= \int_0^1 f_w(\xi) f_\varphi(\xi)\xi d\xi, \quad a_6 = \int_0^1 f_w(\xi)\xi d\xi,
\end{aligned} \tag{31}$$

where $\xi = r/R$ is the normalized radial coordinate. Rearranging Equations 28–30 and using $f_w(1) = 0$, we have:

$$a_1 R^2\frac{dw_c'^2}{dz} + a_1 R^2 w_c'^2\frac{d}{dz}(\ln\rho) + a_1 w_c'^2\frac{dR^2}{dz} = a_2 B_c' R^2 - w_c'^2 R f_\tau(1), \tag{32}$$

$$\frac{3}{4}a_3 R^2 w_c'\frac{dw_c'^2}{dz} + \frac{1}{2}a_3 w_c'^3 R^2\frac{d}{dz}(\ln\rho) + \frac{1}{2}a_3 w_c'^3\frac{dR^2}{dz} = a_4 w_c' B_c' R^2 - a_5 R w_c'^3 \tag{33}$$

$$\frac{d\varphi_c'}{dz}+\varphi_c'\left[\frac{1}{w_c'}\frac{dw_c'}{dz}+2\frac{1}{R}\frac{dR}{dz}+\frac{d}{dz}(\ln\rho)\right]=-\frac{a_6}{a_\varphi}\frac{\partial\overline{\varphi}}{\partial z}-\frac{1}{R}\varphi_c'\frac{j_\varphi(1)}{a_\varphi}+\frac{1}{a_\varphi w_c R^2}J_c^\varphi. \tag{34}$$

In Equations 34, the term $(1/w_c')dw_c'/dz$ represents the dynamical (or buoyancy–driven) entrainment. Multiplying Equation 32 with $a_4 w_c'$ and Equation 33 with a_2 and, by combining them, we can obtain a relation for the dynamical entrainment, as:

$$\frac{1}{w_c'}\frac{dw_c'}{dz}=\frac{a_2a_5-a_4f_\tau(1)}{2a_1a_4-3a_2a_3/2}\frac{1}{R}-\frac{a_1a_4-a_2a_3/2}{a_1a_4-3a_2a_3/4}\frac{1}{R}\frac{dR}{dz}-\frac{a_1a_4-a_2a_3/2}{2a_1a_4-3a_2a_3/2}\frac{d(\ln\rho)}{dz}. \tag{35}$$

Substituting Equation 35 in Equation 34, after some arrangements, Equations 32 and 34 becomes:

$$\frac{dw_c'^2}{dz}=\frac{a_2}{a_1}B_c'-\left[\frac{\eta_1}{R}+2\frac{d(\ln R)}{dz}+\frac{d(\ln\rho)}{dz}\right]w_c'^2, \tag{36}$$

$$\frac{d\varphi_c'}{dz}=\frac{1}{a_\varphi w_c' R^2}J_c^\varphi-\frac{a_6}{a_\varphi}\frac{\partial\overline{\varphi}}{\partial z}-\left[\frac{\eta_2}{R}+\eta_3\frac{d(\ln R)}{dz}+\eta_4\frac{d(\ln\rho)}{dz}\right]\varphi_c', \tag{37}$$

where the coefficients $\eta_1-\eta_4$ are given by:

$$\eta_1=\frac{f_\tau(1)}{a_1},\quad \eta_2=\frac{a_2a_5-a_4f_\tau(1)}{2a_1a_4-3a_2a_3/2}+\frac{j_\varphi(1)}{a_\varphi},\quad \eta_3=2-\frac{a_1a_4-a_2a_3/2}{a_1a_4-3a_2a_3/4},\quad \eta_4=1-\frac{a_1a_4-a_2a_3/2}{2a_1a_4-3a_2a_3/2}. \tag{38}$$

For the buoyancy we may write:

$$\frac{dB_c'}{dz}=-N^2-\left[\frac{\eta_2}{R}+\eta_3\frac{d(\ln R)}{dz}+\eta_4\frac{d(\ln\rho)}{dz}\right]B_c'. \tag{39}$$

Multiplying Equation (32) with $3w_c/(2a_1b)$ and Equation (33) with $2/(a_3b)$ and combining them, we can obtain a relation for the plume radius, as:

$$\frac{dR}{dz}=\eta_5\frac{B_c'R}{w_c'^2}+\eta_6-\frac{R}{2}\frac{d(\ln\rho)}{dz}, \tag{40}$$

where the coefficients η_5 and η_6 are given by:

$$\eta_5=\left(\frac{3a_2}{2a_1}-\frac{2a_4}{a_3}\right),\quad \eta_6=\left(\frac{2a_5}{a_3}-\frac{3f_\tau(1)}{2a_1}\right). \tag{41}$$

The system of Equations 36, 37, 39 and 40 can be solved numerically by the parent numerical model, obtaining

thus the convective variables, and therefore, the convective source terms, if the radial coefficients and the boundary conditions are provided. However, due to the non–linear character of the system of equations, the vertical resolution of the parent model could be too small to be able to produce accurate values for these terms. Of course, one should perform a convergence test before implementing this system of equations in a numerical model. This problem may be avoided by finding approximate analytical solutions, which may be used to describe the convective flow between the vertical grids (z_k and z_{k+1}) of the parent model, where the index k represents the k-th vertical level of the numerical model. Such solutions are presented in the Appendix B.

The analytical solutions are even more useful when the dry plumes originating from the mixed layer become saturated and form shallow or deep convection. As it is often considered, between the top of the mixed layer and the lifting condensation level there is an inversion layer called the transition layer (Betts, 1976; Neggers et al., 2006; Albright et al., 2022). The depth of the transition layer may be smaller than the vertical resolution of the weather or climate numerical model. For this reason, some EDMF schemes assume a parameterization for the number of dry plumes that overshoot the transition layer and form cumulus clouds (Sakradzija et al., 2016). However, considering a stochastic variability for the plumes in a given grid box, this kind of parameterization is no longer needed, since the number of plumes that overshoot the transition layer forming cumulus clouds can be obtained analytically.

The system of Equations 36 and 37 can be brought into a form equivalent with the entraining plume model, if one considers the same assumptions as the ones made in the entraining plume model, namely, top–hat profiles and the Boussinesq approximation. For top–hat profiles we obtain the following values for the radial coefficients: $a_1 = a_2 = a_3 = a_4 = a_\varphi = a_6 = 1$, $a_5 = \eta_1 = f_\tau(1)$, $\eta_2 = j_\varphi(1)$, $\eta_3 = \eta_4 = 0$, $\eta_5 = -1/2$ and $\eta_6 = f_\tau(1)/2$. Therefore, assuming top–hat profiles and the Boussinesq approximation, and combining Equation 36 with Equation 40, we obtain:

$$\frac{dw_c'^2}{dz} = 2B_c' - \frac{3}{2}\frac{f_\tau(1)}{R}w_c'^2, \tag{42}$$

$$\frac{d\varphi_c'}{dz} = \frac{1}{w_c' R^2}J_c^\varphi - \frac{\partial\overline{\varphi}}{\partial z} - \frac{j_\varphi(1)}{R}\varphi_c'. \tag{43}$$

Using that for top–hat profiles $\varphi_c' = \varphi_c - \overline{\varphi}$, one may see that for the conserved variables, for which $J_c^\varphi = 0$, the system on Equations 42 and 43 is mathematically equivalent with the entraining plume model if $\epsilon = j_\varphi(1)/R$, a = 1, and b = $(3/4)f_\tau(1)/j_\varphi(1)$. Even so, the energy–consistent plume model is still a generalisation of the entraining plume model since an additional equation for the plume radius is obtained. Therefore, closure for the radius is required only for the dry plumes in the surface layer. Note that the equation of the plume radius is obtained by combining the momentum equations with the equation for the kinetic energy, and thus, it is a consequence of the conservation of energy. Thus, the plume is energy–consistent, since it evolves such that it conserves its momentum, energy, and buoyancy, in contrast with the entraining plume model which is governed only by the conservation of momentum and buoyancy, in which there is a prescribed radial velocity (entrainment). In our formulation, rather than prescribing the radial velocity based on the entrainment hypothesis or LES results, we obtain the radial velocity from the continuity equation.

4.2 | Convective radial velocity

Finally, the convective radial velocity u_r' is obtained from the convective–scale continuity Equation 20, as:

$$u_r' = -\frac{1}{r\rho}\frac{d}{dz}\left[\int_0^r \rho w' r dr\right], \tag{44}$$

where we used that $u_r'(z, r = 0) = 0$, and performing the integral, we obtain:

$$u_r' = -\frac{1}{r\rho}\frac{d}{dz}\left[\rho w_c R^2 \int_0^{r/R} f_w(\xi)\xi d\xi\right], \tag{45}$$

where $\xi = r/R$. If we consider that between two consecutive vertical levels the plume radius remains approximately constant, then we can consider in a first approximation that Equation 45 can be written as:

$$u_r' = u_c' f_u\left(\frac{r}{R}\right), \tag{46}$$

where the characteristic radial velocity u_c is given by:

$$u_c' = \frac{1}{\rho}\frac{d}{dz}\left[\rho w_c R\right] \tag{47}$$

and the radial function f_u is given by:

$$f_u\left(\frac{r}{R}\right) = -\frac{R}{r}\int_0^{r/R} f_w\left(\xi\right)\xi d\xi. \tag{48}$$

This expression is only valid as an approximation between two consecutive vertical levels since R given by Equation 40 is not constant, and thus, R must be updated at every level before computing the convective radial velocity.

Therefore, we have all the necessary terms for obtaining the convective contribution to the subgrid convective fluxes.

4.3 | Radial profiles and turbulent fluxes closure

As one may see, the closing problem of the presented energy–consistent plume model consists in the specification of the radial coefficients that comes from the integration of the radial profiles of the convective variables. A very simple choice will be to assume top–hat profiles, as is already considered in the existing parametrization schemes. If a top–hat is considered, then, in order to respect the condition $\overline{\varphi'} = 0$, we must have:

$$\varphi' = \begin{cases} \varphi_c' & 0 \le r \le R \\ -\frac{\pi R^2}{L_{x1}L_{x2} - \pi R^2}\varphi_c' & R < r < \infty \end{cases} \tag{49}$$

In the mass–flux formulation it is assumed that $\pi R^2/(L_{x1}L_{x2} - \pi R^2) \ll 1$, since it is assumed that the fractional area occupied by the convection is very small in every grid box, and thus, $\varphi' \approx 0$ for $r > R$.

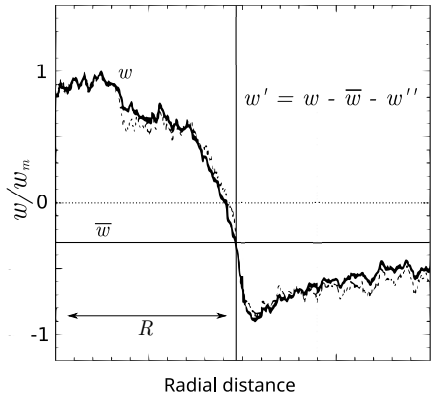

FIGURE 1 The radial profile of the updraft velocity of a cumulus cloud. Based on the airborne measurements of Mallaun et al. (2019), and adapted from Figure 13 of their study.

However, more realistic radial profiles can be considered following numerical simulations or airborne measurements. In Figure 1, a possible choice for the radial profile of the updraft velocity is schematically presented. In this graph, w_m is the maximum vertical velocity of a cumulus cloud. The scheme is based on the airborne measurements of Mallaun et al. (2019) for warm shallow cumulus clouds. Following the measurements and numerical simulations of the radial profiles of the flow in clouds and dry plumes, we may consider that the convective vertical velocity is given by a profile similar to the one presented in Figure 1 in which the vertical velocity goes to the mean state $\overline{w}$ far from the convective plume, which means that $w'(z, r \to \infty) = 0$. Pinsky et al. (2021) showed that a scale separation between the convective and turbulent motion can be considered for nonprecipitating cumulus clouds if one assumes the following radial profile of the updraft velocity:

$$w' = w'_c \left(1 - \frac{r^2}{R^2}\right) \exp\left(-\frac{r^2}{R^2}\right), \tag{50}$$

which respects the condition $\overline{w'} = 0$ and is able to reproduce the observed subsidising shells around the updraft region, being also in agreement with the airborne measurements of Mallaun et al. (2019) or with the large eddy simulations of Savre (2021). However, for the scalar φ different profiles have been found (Gu et al., 2021), and thus, we do not consider a universal profile for any scalar, but just to close the system one may assume the top–hat profile (Equation 49). Note that even if a profile such as given in Equation 49 does not go to zero in the far–field, since we assume that $w'(z, r \to \infty) = 0$ any product $w'\varphi'$ will asymptotically become zero in the far–field. This condition will become important when performing the subgrid averaging.

4.3.1 | The asymptotic behavior of w'

Let us consider that the convective vertical velocity w' follows a top–hat profile, such as:

$$w' = \begin{cases} w'_c & 0 \leq r \leq R \\ -\frac{\pi R^2}{L_{x1}L_{x2}-\pi R^2} w'_c & R < r < \infty \end{cases} \tag{51}$$

Substituting this profile in Equation (48) we obtain the radial profile of the radial velocity as:

$$f_u\left(\frac{r}{R}\right) = \begin{cases} -\frac{r}{2R} & 0 \leq r \leq R \\ \frac{1}{2}\frac{\pi R^2}{L_{x1}L_{x2}-\pi R^2}\frac{r}{R} & R < r < \infty \end{cases} \tag{52}$$

As one may see, under a top–hat profile for the vertical velocity, the convective radial velocity goes to infinity far from the convective updraft. This behavior is clearly nonphysical, and thus, we argue that a top–hat profile for w' can be used only if the convective radial velocity is completely neglected. Furthermore, for any profile in which $w'(z, r \to \infty) \neq 0$, will correspond a convective radial velocity that goes to infinity in the far field. Therefore, we must consider the asymptotic behavior $w'(z, r \to \infty) = 0$ in order to obtain a complete parameterization in which the subgrid fluxes containing the convective radial velocity are not neglected. This asymptotic behavior can be also observed from recent measurements and numerical simulations (Mallaun et al., 2019; Griewank et al., 2020; Gu et al., 2021; Savre, 2021).

4.3.2 | Turbulent fluxes closure

The radial turbulent fluxes may be closed by following the mixing length model:

$$\tau_w = -C_{mix}\, l_{mix}^2(z) \left|\frac{\partial w'}{\partial r}\right| \frac{\partial w'}{\partial r}, \tag{53}$$

$$\tau_\varphi = -C_{mix,\varphi}\, l_{mix}^2(z) \left|\frac{\partial w'}{\partial r}\right| \frac{\partial \varphi'}{\partial r}, \tag{54}$$

where C_{mix} and $C_{mix,\varphi}$ are the mixing constants for w' and φ', respectively, and l_{mix} is the mixing length. Considering that $l_{mix} = R$, Kewalramani et al. (2022) based on large–eddy simulation results found $C_{mix} = 0.034$ and $C_{mix,\varphi} = 0.041$, but probably for the dry and moist atmospheric convection other coefficients might be considered, and thus, future work is required in order to find the appropriate coefficients for the dry, shallow, and deep convective plumes. Therefore, following the mixing length closure with $l_{mix} = R$, the radial profiles of the turbulent fluxes becomes:

$$f_\tau(\xi) = -C_{mix} \left|\frac{df_w(\xi)}{d\xi}\right| \frac{df_w(\xi)}{d\xi}, \tag{55}$$

$$j_\varphi(\xi) = -C_{mix,\varphi} \left|\frac{df_w(\xi)}{d\xi}\right| \frac{df_\varphi(\xi)}{d\xi}, \tag{56}$$

where $\xi = r/R$. Also, note that Kewalramani et al. (2022) also neglects the pressure redistribution term, but they still obtain very good agreements with LES. This might be because the contribution of the pressure term is implicitly considered in the coefficients C_{mix} and $C_{mix,\varphi}$. However, one may also consider the pressure redistribution terms in an explicit way in the above–discussed energy–considered plume model, but this will require additional closure. Thus, tuning the energy–consistent plume model must be made before building a parameterization scheme, which is beyond the scope of this work.

5 | THE SUBGRID FLUXES

We consider that in a given grid–box with the area $L_x L_y$ we can have a number of n plumes described by the Equations 36, 37 and 40. We assume that for every plume there is a corresponding subgrid–box with an area $l_{x1} l_{x2}$ large enough such that $\langle w' \rangle = \langle u_i' \rangle = \langle \varphi' \rangle = 0$, where l_{xi} is the horizontal dimension of the small subgrid–box in the i-th direction, and where we define the averaging operator $\langle \cdot \rangle$ as:

$$\langle \cdot \rangle = \frac{1}{l_{x1} l_{x2}} \int_{-l_{x1}/2}^{+l_{x2}/2} \int_{-l_{x2}/2}^{+l_{x2}/2} dx_1 dx_2. \tag{57}$$

It follows thus that we have:

$$\overline{(\cdot)} = \frac{1}{n} \sum_{k'=1}^{n} \langle \cdot \rangle_{k'}, \tag{58}$$

where we index with k' the plumes in the given grid–box.

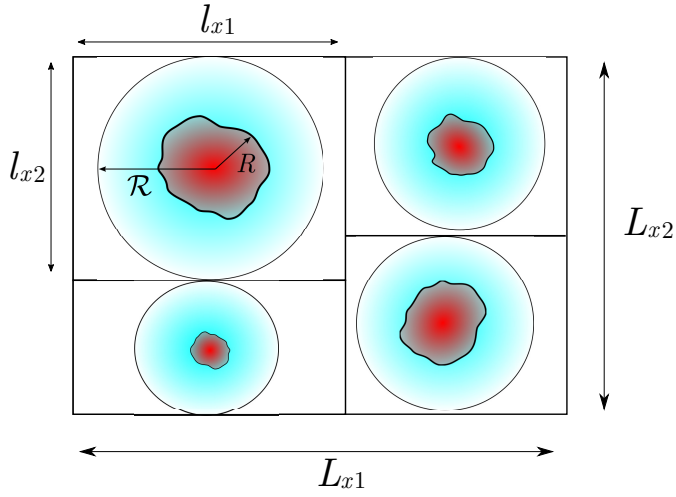

FIGURE 2 The sub–grid scheme for a case with four convective plumes of different dimensions. With red is represented the updraft area, characterized by a positive w', and with blue the subsidising shells are characterized by a negative w'. The vertical velocity w gradually transitions to the mean state denoted by white color.

In Figure 2 it is illustrated a schematic draw for a case in which there are four convective plumes in a grid–box. Since we consider that the plumes are axisymmetric and we prescribe the convective–scale variables in cylindrical coordinates, it is convenient to define a radial distance $\mathcal{R}$ inside every small subgrid–box, defined from the center of the plume, large enough such that $w' \approx 0$ and $u'_r \approx 0$ at $r = \mathcal{R}$. Therefore, we can consider the following approximation:

$$\langle w'\varphi' \rangle \approx \frac{1}{l_{x1} l_{x2}} \int_0^{\mathcal{R}} w'\varphi' r\, dr \approx \frac{1}{l_{x1} l_{x2}} \int_0^{\infty} w'\varphi' r\, dr. \tag{59}$$

Considering that the convective plume is placed in the center of their corresponding subgrid–box $l_{x1} l_{x2}$, the component u'_i of the horizontal convective flow produced by one plume is given by:

$$u'_i = u'_c f_u \left(\frac{\sqrt{x_i'^2 + x_j'^2}}{R} \right) \frac{x'_i}{\sqrt{x_i'^2 + x_j'^2}}, \tag{60}$$

with $x'_i \in [-l_{xi}/2; l_{xi}/2]$ and $i \neq j$. Thus, u'_i is an odd function with respect of $x'_i = 0$, which means that if the plume is placed in the center of the box, $\langle u'_i \rangle = 0$. Therefore, the assumed condition $\overline{u'_i} = 0$ is respected. Note that u'_r cannot have positive and negative values at the same height at the same time. In other words, a single plume cannot produce both a convergence and a divergence at a given height and time, since this behavior will be unphysical. For exactly this reason, the imposed condition $\overline{u'_i} = 0$ is respected only if u'_i is an odd function. As a result, $\langle u'_i w' \rangle = \langle u'_i \varphi' \rangle = \langle u'_i u'_j \rangle = 0$ (for $i \neq j$), since u'_i is an odd function and w' and φ' are even functions with respect of $x'_i = 0$. In addition, we have:

$$\langle u_i'^2 \rangle \approx c_1 \frac{R^2}{2 l_{x1} l_{x2}} u_c'^2, \tag{61}$$

if $l_{x1} \approx l_{x2}$, and

$$\langle w'^2 \rangle \approx c_2 \frac{R^2}{l_{x1} l_{x2}} w_c'^2, \tag{62}$$

$$\langle \varphi' w' \rangle \approx c_3 \frac{R^2}{l_{x1} l_{x2}} \varphi'_c w'_c, \tag{63}$$

where the radial coefficients $c_1 - c_3$ are given by:

$$c_1 \approx \int_0^{\infty} f_u^2(\xi)\, \xi d\xi, \quad c_2 \approx \int_0^{\infty} f_w^2(\xi)\, \xi d\xi, \quad c_3 \approx \int_0^{\infty} f_w f_\varphi(\xi)\, \xi d\xi. \tag{64}$$

Using Equation 58, for the sub–grid flux $\overline{\varphi^* w^*}$ we obtain:

$$\overline{\varphi^* w^*} = \frac{1}{n}\sum_{k'=1}^{n}\langle \varphi'_{k'} w'_{k'}\rangle_{k'} + \frac{1}{n}\sum_{k'=1}^{n}\langle \varphi'' w''\rangle_{k'} + \frac{1}{n}\sum_{k'=1}^{n}\left(\langle \varphi'_{k'} w''\rangle_{k'} + \langle \varphi'' w'_{k'}\rangle_{k'}\right). \tag{65}$$

Since $\langle \varphi' \rangle = \langle \varphi'' \rangle = \langle w' \rangle = \langle w'' \rangle = 0$ and the convective variables have different forms and dimensional scales than the turbulent ones (Pinsky et al., 2021; Pinsky and Khain, 2023) (see also Figure 1), we can consider that $\langle \varphi' w'' \rangle = \langle \varphi'' w' \rangle = 0$. And writing the flux $\langle \varphi'_{k'} w'_{k'} \rangle$ in terms of the mass flux $M'_{k'} = \rho \sigma_{k'} w'_{c,k'}$, in which $\sigma_{k'} = c_3 R^2_{k'}/L_{x1}L_{x2}$ is the equivalent fractional area occupied by the k'-th plume, we obtain:

$$\rho\overline{\varphi^* w^*} = \sum_{k'=1}^{n} M'_{k'} \varphi'_{c,k'} + \rho\overline{\varphi'' w''}, \tag{66}$$

where we used that $l_{x1} l_{x2} \approx L_{x1} L_{x2}/n$. Therefore, one may see that if we consider an eddy–diffusivity closure for the turbulent flux $\overline{\varphi'' w''}$, then for the subgrid flux $\overline{\varphi^* w^*}$ we recover the eddy–diffusivity mass–flux (EDMF) formulation. For the rest of the subgrid fluxes, following the same considerations as before, we have:

$$\overline{w^* u_i^*} = \overline{w'' u_i''}, \tag{67}$$

$$\overline{\varphi^* u_i^*} = \overline{\varphi'' u_i''}, \tag{68}$$

$$\rho\overline{w^{*2}} = \sum_{k'=1}^{n} \frac{c_2}{c_3} M'_{k'} w'_{c,k'} + \rho\overline{w''^2}, \tag{69}$$

$$\overline{u_i^{*2}} = \sum_{k'=1}^{n} c_1 \frac{R^2_{k'}}{2 l_{x1} l_{x2}} u'^2_{c,k'} + \overline{u_i''^2}. \tag{70}$$

$$\overline{u_i^* u_j^*} = \overline{u_i'' u_j''}, \tag{71}$$

with $i \neq j$.

Note that in the EDMF parameterization the fluxes $\overline{\varphi^* u_i^*}$ and $\overline{u_i^* u_j^*}$ are neglected and $\overline{w^* u_i^*}$ may also contains a convective term considering the wind component as a conservative variable (e.g. Hourdin et al., 2002; Rio and Hourdin, 2008), or it is neglected altogether. Thus, the present parameterization generalizes the EDMF formulation not only by the more generic convective radial profiles and a more generic plume model but also by the subgrid fluxes. These differences appear since we consider that u'_i is an odd function with respect of the center of the plume, which is a necessary condition in order to respect the assumed condition $\overline{u'_i} = 0$. However, in the mass–flux formulation even if

$\overline{u_i'} = 0$ is considered, the behavior of the convective radial velocity is overlooked, probably because the condition $\overline{u_i'} = 0$ is respected as an approximation from the beginning since the mass–flux formulation assumes a very small fractional area occupied by the convection in every grid box. Therefore, one may see that in our formulation, although we make some assumptions regarding the difference between the plume area and the grid box area, we do not need to consider the assumption that the fractional area occupied by the convection in every grid box is very small. The resolution limitation of our formulation is discussed in Section 6. Note, in addition, that we obtain the subgrid fluxes in the same way even if we make the assumptions of the mass–flux formulation of a top–hat profile for updraft velocity and a small fractional area occupied by the convection in every grid box, since in this case the condition $w'(z, r \to \infty) = 0$ is still respected.

6 | MAXIMUM RESOLUTION LIMIT

The maximum resolution is obtained when we only have a single plume in every grid–box. Furthermore, the resolution is limited by the condition $\overline{\varphi'} = 0$, $\overline{w'} = 0$ and $\overline{u_i'} = 0$. Assuming that the plume is placed exactly in the center of the grid box, the condition $\overline{u_i'} = 0$ is respected for any resolution since it is an odd function. However, in reality, the plume may not be located exactly in the center of the grid box, but we can consider that it can be translated to the center if $u_i' \approx 0$ at the boundary of the box (two neighbor plumes are far enough that they do not interact directly, and thus they can be considered isolated). We also assumed that there is a circular area in every box of the plume such that the averaging over the box can be given by Equation 59. Since at the maximum resolution we have $n = 1$ in every grid box, $\langle \cdot \rangle = \overline{(\cdot)}$, and the radius of the circular area is given by $\mathcal{R} = \min(L_{x1}/2, L_{x2}/2)$. It follows thus that for the maximum resolution, we must have $L_{x1} = L_{x2}$. We also had to consider that $\mathcal{R}$ is large enough such that $w' \approx 0$ at $r = \mathcal{R}$. Therefore, the problem reduces to find $\mathcal{R} = L_{x1}/2 = L_{x2}/2$ such that $\overline{\varphi'} = 0$, $\overline{w'} = 0$, $w'(z, r = \mathcal{R}) \approx 0$ and $u_r'(z, r = \mathcal{R}) \approx 0$. The condition $\overline{\varphi'} = 0$ can be easily respected by the way it is defined with respect to the mean $\overline{\varphi}$, such is for example in Equation 49. Choosing for w' a top–hat profile such as in Equation 51 gives that the condition $w'(z, r = \mathcal{R}) \approx 0$ is respected only if the fractional area occupied by the convection in every grid box is very small. In this case, we recover the assumptions of the mass–flux formulation, but our development is still the same. However, if one chooses a profile based on measurements and observations in which it can be considered in a good approximation that $w'(z, r \to \infty) = 0$, then one could find that the fractional area occupied by the convection is not required to be very small in every grid box. Thus, once one chooses the convective radial profiles, one can also study the resolution limit of the parent numerical model in which the parametrization is implemented. Only as an exemplification, we discuss here the resolution limit for a profile given by Equation 50. For this profile, for the radial profile of the radial velocity we obtain:

$$f_u\left(\frac{r}{R}\right) = \frac{1}{2}\frac{r}{R}\exp\left(-\frac{r^2}{R^2}\right). \tag{72}$$

From the graphical representation of $f_w(r/R)$ and $f_u(r/R)$ presented in Figure 3, we can consider that the minimum radius $\mathcal{R}$ for which the above–discussed conditions are met is $\mathcal{R} = 2R$, which gives a minimum resolution of $L_{x1} = L_{x2} = 4R$, corresponding to a maximum fractional area occupied by the convection σ_m in a grid box of about 0.2. Therefore, if one considers the radial profile given by Equation 50 the condition of a fractional area occupied by the convection can be a little bit relaxed. In the next section, we will show how under the present formulation, this condition can be relaxed even further.

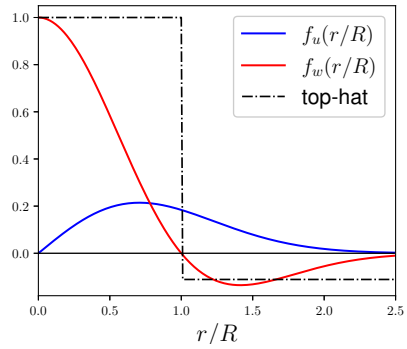

FIGURE 3 The graphical representation of the radial profiles of the convective vertical velocity and convective radial velocity, and the corresponding top–hat profile (dash–dotted line) for a fractional area occupied by the plume of 0.1.

7 | PUSHING THE RESOLUTION LIMIT

Until this point, we only presented the case in which there is a clear scale separation between the convection and the mean grid–box resolved flow. However, we can extend our formulation for horizontal resolutions similar to the radius of the convective plumes by only considering a few modifications.

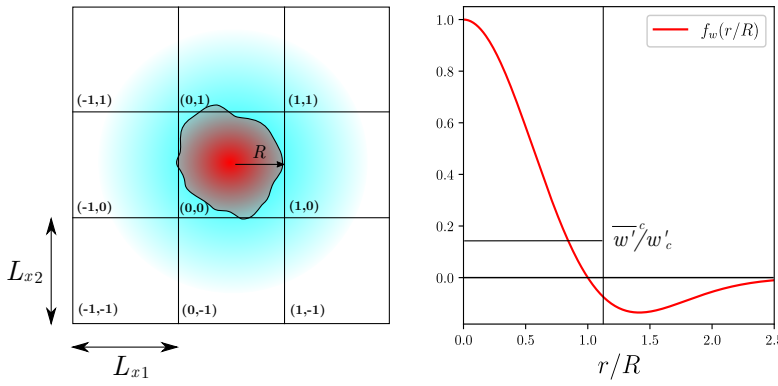

FIGURE 4 Schematic view of a plume in a grid for a case in which the diameter of the plume is equal to the horizontal resolution of the host numerical model (left), and the graphical representation of the radial profile of the convective vertical velocity, as well as the associated mean grid–box convective vertical velocity $\overline{w'}^c$ (right).

Let us consider a situation in which $L_{x1} = L_{x2} = 2R$, corresponding to a fractional area occupied by the convection of $\pi/4$, as illustrated in Figure 4. For such a situation, the convective scale variables w' and φ' are no longer a fluctuation from the mean variables $\overline{w}$ and $\overline{\varphi}$, and thus, the convective scale variables need to be redefined. We can perform this procedure without changing the plume model if we replace the mean variable $\overline{\varphi}$ with a large–scale

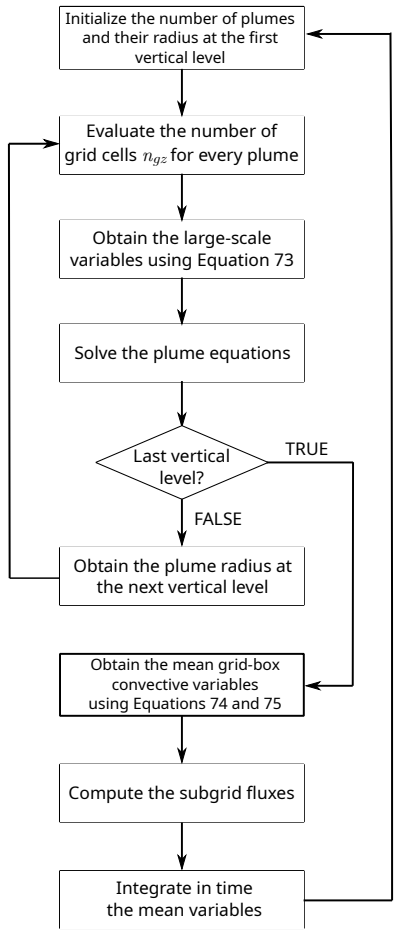

FIGURE 5 Flowchart of the formulation in the gray–zone.

variable $\overline{\overline{\varphi}}$ (similar for w and u_i) in the plume model, where $\overline{\overline{(\cdot)}}$ is defined as the average over the grid cells in which $\overline{w'} \not\approx 0$. This procedure needs to be considered for every plume at a given vertical level. Thus, we have:

$$\overline{\overline{\varphi}} = \sum_{\iota=1}^{n_{gz}} \overline{\varphi}_\iota, \tag{73}$$

where n_{gz} is the number of grid cells for which $\overline{w'} \not\approx 0$ at a given vertical level associated with a single plume, and ι is a summation index. For the case illustrated in Figure 4 we have $n_{gz} = 9$. Therefore, w no longer goes to $\overline{w} + w''$ far from the plume, but it rather goes to $\overline{\overline{w}} + w''$. As a result, we need to change the convective variable φ' with $\varphi' - \overline{\varphi'}^c$ (similar for w' and u_i'), in which $\overline{\varphi'}^c$ is the mean grid–box value of the convective variable φ', defined as:

$$\overline{\varphi'}^c = \frac{1}{L_{x1} L_{x2}} \int_0^{\Re} \varphi' r dr, \tag{74}$$

for the grid–box in which the center of the plume is present, and

$$\overline{\varphi'}^c = \frac{1}{(n_{gz} - 1) L_{x1} L_{x2}} \int_{\Re}^{\infty} \varphi' r dr, \tag{75}$$

for the neighbor grid–boxes, and where $\Re$ is an equivalent radius to the grid–box area (the radius a circular grid would have such that its area would be equal with the area of the grid–box), defined as $\Re = (L_{x1} L_{x2}/\pi)^{1/2}$. For the case illustrated in Figure 4, $\Re \approx 1.13R$. The flowchart of the scheme is presented in Figure 5. Note that if there is a scale separation between convection and grid–box flow, then $n_{gz} = 1$ and $\overline{\overline{\varphi}} = \overline{\varphi}$, which further gives that $\int_0^{\Re} \varphi' r dr \approx \int_0^{\infty} \varphi' r dr = 0$. Therefore, the subgrid flux $\overline{w^* \varphi^*}$ is given by (similar to the other ones):

$$\overline{w'\varphi'} = \frac{1}{L_{x1} L_{x2}} \int_0^{\Re} (w' - \overline{w'}^c)(\varphi' - \overline{\varphi'}^c) r dr = \frac{1}{L_{x1} L_{x2}} \left[\int_0^{\Re} w'\varphi' r dr - \overline{w'}^c \overline{\varphi'}^c \right], \tag{76}$$

for the grid–box in which the center of the plume is present, and

$$\overline{w'\varphi'} = \frac{1}{(n_{gz} - 1) L_{x1} L_{x2}} \int_{\Re}^{\infty} (w' - \overline{w'}^c)(\varphi' - \overline{\varphi'}^c) r dr = \frac{1}{(n_{gz} - 1) L_{x1} L_{x2}} \left[\int_{\Re}^{\infty} w'\varphi' r dr - \overline{w'}^c \overline{\varphi'}^c \right], \tag{77}$$

for the neighbor grid–boxes. In the limit $\Re \gg R$ we have $\overline{w'}^c \approx \overline{\varphi'}^c \approx 0$, and thus, we recover the flux given by Equation 66. On the other hand, in the limit $\Re \ll R$ we have $(w' - \overline{w'}^c) \approx (\varphi' - \overline{\varphi'}^c) \approx 0$, and thus, the convective contribution to the subgrid fluxes vanishes and the convection becomes fully resolved. Note that for a fractional area occupied by a plume in a given grid box of 1, if one uses a top–hat profile, as in the mass–flux formulation, then the convection becomes resolved. However, if more realistic radial profiles are considered for the convective variables, then even at such a resolution the convection is not fully resolved, which could improve the numerical simulations running in the gray–zone of convection. Moreover, since in the energy–consistent plume model the plumes are allowed to grow with the height, a plume can be completely parameterized at a given vertical level, partially resolved at the next level, and become fully resolved at higher levels.

It should be also noted that Equations 75 and 77 correspond for the simple case where all neighboring grid cells are treated equally. Of course, depending on the geometry of the parent numerical model, one can consider that not all neighboring grid cells are equal, and thus, Equations 75 and 77 can be adjusted by simply adding a weight for each neighboring grid cells.

If there is no scale separation between the convection and the grid–box flow, then the convective components of the horizontal momentum fluxes $\overline{w'u_i'}$ are no longer necessarily zero, as obtained above. To obtain the momentum flux $\overline{w'u_i'}$ for the case illustrated in Figure 4, we must first obtain $\overline{u_i'}$ in every grid–box displayed in Figure 4. For the grid–box in which the plume center is present, because u_i' is an odd function with respect to the box center, $\overline{u_i'}^c = 0$. However, in the neighboring boxes, u_i' is no longer necessarily an odd function. In the grid denoted with (1,0) on the schematic presented in Figure 4, $\overline{u_i'}^c$ is given by:

$$\overline{u_i'}^c = \frac{1}{L_{x1}L_{x2}} \int_{+L_{x1}/2}^{+3L_{x1}/2} \int_{-L_{x2}/2}^{+L_{x2}/2} u_i' dx_1 dx_2, \tag{78}$$

where u_i' is given by Equation 60. Note that for the grid–box (1,0), $\overline{u_2'}^c = 0$, as u_2' is an odd function with respect of the $x_2 = 0$ axis. For all grid–boxes, we can write $\overline{u_i'}^c$ in a more condensed form if we denote with (m,n) the grid–boxes, where $m, n = \overline{-1, 1}$. Thus, for a grid–box (m,n), we have:

$$\overline{u_i'}^c = \frac{1}{L_{x1}L_{x2}} \int_{-\frac{L_{x1}}{2}+mL_{x1}}^{+\frac{L_{x1}}{2}+mL_{x1}} \int_{-\frac{L_{x2}}{2}+nL_{x2}}^{+\frac{L_{x2}}{2}+nL_{x2}} u_i' dx_1 dx_2, \tag{79}$$

where $\overline{u_1'}^c = 0$ if $m = 0$, and $\overline{u_2'}^c = 0$ if $n = 0$. The integrals that do not give zero can be easily performed after the radial profiles are prescribed. The horizontal subgrid flux $\overline{w'u_i'}$ is thus given for the grid–box (m,n) by:

$$\overline{w'u_i'} = \frac{1}{L_{x1}L_{x2}} \left[\int_{-\frac{L_{x1}}{2}+mL_{x1}}^{+\frac{L_{x1}}{2}+mL_{x1}} \int_{-\frac{L_{x2}}{2}+nL_{x2}}^{+\frac{L_{x2}}{2}+nL_{x2}} w'u_i' dx_1 dx_2 - \overline{w'}^c \overline{u_i'}^c \right], \tag{80}$$

which also gives $\overline{w'u_1'} = 0$ if $m = 0$, and $\overline{w'u_2'} = 0$ if $n = 0$. The rest of the subgrid fluxes depending on u_i' (e.g. $\overline{\varphi'u_i'}$) are computed similarly with $\overline{w'u_i'}$.

It might seem that when the fractional area occupied by a given plume is equal to 1, the grid–mean property should be identical to the updraft plume property of the diagnostic plume model. However, this is not necessarily the case for the following reason: both the grid–mean property and the diagnostic updraft plume property are merely approximate solutions of a real updraft, and there is no reason to believe that they are identical. For the case when the fractional area occupied by a given plume is equal to 1, without the subgrid convective term, the grid–mean flow is just a zero–order approximation of the updraft flow (due to the poor representation of mixing between the updraft and the environment), while the convective fluxes, modeled by the diagnostic plume model, provide a first–order correction to the resolved flow. However, even with this correction, we cannot expect the mean–flow to become identical to the convective flow of the idealized plume model.

8 | SUMMARY AND CONCLUSIONS

In this work we present a theoretical framework for the parameterization of subgrid–scale convection and turbulence following the grid–box averaging technique that generalizes the eddy–diffusivity mass–flux formulation. The fundamental difference between our development and the mass–flux formulation is that we do not assume the subgrid to be composed of two distinct fluids, namely, top–hat convective plume which occupies a very small fractional area, and an environment, which is assumed to be described by the mean state. We rather assume that the subgrid components are represented by convective and turbulent variables, where the convection is described by round plumes that gradually transition into the environmental state, defined at infinity. This treatment provides a more general framework than the mass–flux formulation since more realistic radial profiles for the convective plumes can be considered, and the condition of a very small fractional area occupied by convection is relaxed. Therefore, our framework is might more suitable for the development of stochastic scale–aware parameterizations at the convective gray zone. The convective and turbulent contributions to the subgrid fluxes are obtained in a unified way, without making additional assumptions. In order to obtain the subgrid fluxes, the only required assumption is that the convective vertical velocity will transition to the mean state (in other words: the vertical velocity of the environment, defined at infinity, is approximately equal to the mean vertical velocity), and this assumption replaces the condition of a very small fractional area occupied by the convection. However, it is shown that for assumed top–hat profiles our formulation becomes similar with the mass–flux formulations since a top–hat plume will transition to the mean state only if the fractional area occupied by the convection is very small. The maximum resolution limit of our formulations depends thus on the assumed radial profile. This problem is discussed in Section 6. Furthermore, the extension of the present formulation for high resolutions is presented in Section 7, where it is shown that, if proper radial profiles are assumed, then the convection can be partially parameterized and partially resolved even for a horizontal grid–spacing similar with the horizontal dimension of the convective plumes, which has the potential to further improve the numerical simulations at the convective gray–zone since the LES studies showed that even at such a high resolution the convection cannot be adequately resolved, as discussed in the Introduction.

We should reiterate the difference between our formulation and the mass–flux formulation regarding the definition of the environment, in order to avoid any confusion. In the mass–flux formulation the environment is defined as the whole fluid outside the convective updrafts (or any other convective elements, if considered). In the present formulation, however, the environment is defined in the asymptotic limit of the convective updraft. Thus, assuming that the mean vertical velocity is equal to the environmental vertical velocity in the present formulation, it is not the same in the mass–flux formulation, where this assumption is not even considered.

It is also shown how the classical entraining plume model can be also generalized by the so–called energy–consistent plume model. In the energy–consistent plume model the convective variables are governed by the conservation of mass, momentum, kinetic energy, and buoyancy, which makes the system of equations to be closed. Furthermore, an equation for the plume radius is obtained, which facilitates the representation of all types of convection in a unified way, since the plume radius, regardless of its type, will be governed by the conservation of the momentum and kinetic energy, as discussed at the end of Section 4. In addition, the differences between the energy–consistent plume model and the entraining plume model for the case of top–hat radial profiles are also discussed in Section 4. Moreover, approximate analytical solutions for the steady–state energy–consistent plume model are obtained in Appendix B. The approximate analytical solutions can be used to model the convective flow between the vertical grids of the parent numerical model if its resolution is too small. Moreover, if a stochastic closure is assumed, the analytical solutions can be used to compute the number of plumes that overshoot the transition layer between the mixed layer and the lifting condensation level, which eliminates the need for additional parameterization for the

number of dry plumes that transform into convective clouds.

Finally, it should be emphasized that here only a general framework is derived, based purely on theoretical considerations, and not a specific parameterization scheme. A parameterization scheme is obtained by choosing the radial profiles for the convective plume and introducing a parameterization for the cloud source terms. In addition, boundary conditions for the convective variables at the initial vertical level are required, and a stochastic variability can be considered. In this work, it is shown how a generalized eddy–diffusivity mass–flux (GEM) formulation can be derived from scratch while keeping the number of required assumptions to as few as possible. It is shown in this way how the EDMF formulation is recovered and exactly what assumptions are required to formulate an EDMF and why. In this sense, the present work also provides a formulation structure of the EDMF parameterization. It should be noted that under the present formulation, many assumptions required by the EDMF formulation can be relaxed, and this allows one to further generalize the formulation by relaxing various approximations made during the derivations presented here. High–resolution large–eddy simulations might provide useful guidelines for such a task.

A | CONVECTIVE PLUME EQUATIONS

Considering a convective plume placed in the center of a cylindrical system of coordinates, the mass continuity, momentum, and advection–diffusion equations are given by:

$$\frac{\partial}{\partial z}(r\rho w) + \frac{\partial}{\partial r}(r\rho u_r) = 0, \tag{81}$$

$$\frac{\partial}{\partial t}(r\rho w) + \frac{\partial}{\partial z}(r\rho w^2) + \frac{\partial}{\partial r}(r\rho u_r w) = r\rho B - \frac{\partial}{\partial z}(rp^*), \tag{82}$$

$$\frac{\partial}{\partial t}(r\rho\varphi) + \frac{\partial}{\partial z}(r\rho\varphi w) + \frac{\partial}{\partial r}(r\rho u_r\varphi) = r\rho F_\varphi, \tag{83}$$

where $w = \overline{w} + w^*$, $u_r = \overline{u_r} + u_r^*$, $B = \overline{B} + B^*$, $\varphi = \overline{\varphi} + \varphi^*$ and $F_\varphi = \overline{F_\varphi} + F_\varphi^*$. Here, u_r represents the radial velocity with respect to the center of the plume in cylindrical coordinates, p^* is the redistribution pressure, and F_φ is the source term of the scalar φ. Substituting $\varphi = \overline{\varphi} + \varphi^*$ in Equation 83 and using the continuity Equation 81, we obtain:

$$\frac{\partial}{\partial t}(r\rho\varphi^*) + \frac{\partial}{\partial z}(r\rho w\varphi^*) + \frac{\partial}{\partial r}\left(r\rho u_r\varphi^*\right) = -r\rho\left[w\frac{\partial\overline{\varphi}}{\partial z} + \frac{\partial\overline{\varphi}}{\partial t}\right] + r\rho F_\varphi. \tag{84}$$

Substituting $w = \overline{w} + w^*$, $u_r = \overline{u_r} + u_r^*$, $B = \overline{B} + B^*$ and $F_\varphi = \overline{F_\varphi} + F_\varphi^*$ and assuming that at the convective scale ($r \sim R$) we can consider that $w \approx w^*$ and $F_\varphi \approx F_\varphi^*$, and thus, the system of Equations 81–83 becomes:

$$\frac{\partial}{\partial z}(r\rho w^*) + \frac{\partial}{\partial r}(r\rho u_r^*) + \frac{\partial}{\partial z}(r\rho\overline{w}) + \frac{\partial}{\partial r}(r\rho\overline{u_r}) = 0, \tag{85}$$

$$\frac{\partial}{\partial t}(r\rho w^*) + \frac{\partial}{\partial z}(r\rho w^{*2}) + \frac{\partial}{\partial r}[r\rho(\overline{u_r} + u^*)w^*] = r\rho B^* - \frac{\partial}{\partial z}(rp^*), \tag{86}$$

$$\frac{\partial}{\partial t}(r\rho\varphi^*) + \frac{\partial}{\partial z}(r\rho w^*\varphi^*) + \frac{\partial}{\partial r}\left[r\rho(\overline{u_r} + u^*)\varphi^*\right] = -r\rho\left[w^*\frac{\partial\overline{\varphi}}{\partial z} + \frac{\partial\overline{\varphi}}{\partial t}\right] + r\rho F_\varphi^*, \tag{87}$$

where we also assumed that $B \approx B^*$. Applying the averaging operator $\overline{(\cdot)}$ on Equation 85 we obtain:

$$\frac{\partial}{\partial z}(r\rho\overline{w}) + \frac{\partial}{\partial r}(r\rho\overline{u_r}) = 0, \tag{88}$$

and therefore, we also have:

$$\frac{\partial}{\partial z}(r\rho w^*) + \frac{\partial}{\partial r}(r\rho u_r^*) = 0. \tag{89}$$

From the continuity equations of the mean and convective variables we see that if $|w^*| \gg |\overline{w}|$, then $|u_r^*| \gg |\overline{u_r}|$, which means that $\overline{u_r} + u_r^* \approx u_r^*$, and substituting $w^* = w' + w''$, $u_r^* = u_r' + u_r''$, $B^* = B' + B''$, $p^* = p' + p''$, and $\varphi^* = \varphi' + \varphi''$, we obtain:

$$\frac{\partial}{\partial z}(r\rho w') + \frac{\partial}{\partial r}(r\rho u_r') + \frac{\partial}{\partial z}(r\rho w'') + \frac{\partial}{\partial r}(r\rho u_r'') = 0, \tag{90}$$

$$\frac{\partial}{\partial t}[r\rho(w' + w'')] + \frac{\partial}{\partial z}[r\rho(w' + w'')^2] + \frac{\partial}{\partial r}[r\rho(u_r' + u_r'')(w' + w'')] = r\rho(B' + B'') - \frac{\partial}{\partial z}\left[r(p' + p'')\right], \tag{91}$$

$$\begin{aligned}&\frac{\partial}{\partial t}[r\rho(\varphi' + \varphi'')] + \frac{\partial}{\partial z}[r\rho(w' + w'')(\varphi' + \varphi'')] + \frac{\partial}{\partial r}\left[r\rho(u_r' + u_r'')(\varphi' + \varphi'')\right] = \\ &-r\rho\left[(w' + w'')\frac{\partial\overline{\varphi}}{\partial z} + \frac{\partial\overline{\varphi}}{\partial t}\right] + r\rho(F_\varphi' + F_\varphi'').\end{aligned} \tag{92}$$

Applying on the system of Equations 90–92 a convective–scale averaging operator $\langle\cdot\rangle_c$, defined in such a way that $\langle\varphi'\rangle_c = \varphi'$, $\langle\overline{\varphi}\rangle_c = \overline{\varphi}$ and $\langle\varphi''\rangle_c = 0$, after some rearrangements, we get:

$$\frac{\partial}{\partial z}(r\rho w') + \frac{\partial}{\partial r}(r\rho u_r') = 0, \tag{93}$$

$$\frac{\partial}{\partial t}(r\rho w') + \frac{\partial}{\partial z}(r\rho w'^2) + \frac{\partial}{\partial r}(r\rho u_r' w') = r\rho B' - \frac{\partial}{\partial z}(rp') - \frac{\partial}{\partial z}[r\rho\langle w''^2\rangle_c] - \frac{\partial}{\partial r}(r\rho\tau_w), \tag{94}$$

$$\frac{\partial}{\partial t}(r\rho\varphi') + \frac{\partial}{\partial z}(r\rho w'\varphi') + \frac{\partial}{\partial r}\left(r\rho u_r'\varphi'\right) = -r\rho w'\frac{\partial\overline{\varphi}}{\partial z} - \frac{\partial}{\partial z}[r\rho\langle w''\varphi''\rangle_c] - \frac{\partial}{\partial r}(r\rho\tau_\varphi) + r\rho F_\varphi', \tag{95}$$

where $\tau_w = \langle u_r'' w''\rangle_c$ is the radial turbulent shearing stress and $\tau_\varphi = \langle u_r''\varphi''\rangle_c$ is the radial turbulent diffusion term of the scalar φ', and where we consider that $|w'(\partial\overline{\varphi}/\partial z)| \gg |\partial\overline{\varphi}/\partial t|$. Also, as it is always assumed in the plumes models, based on dimensional arguments, the terms $\frac{\partial}{\partial z}(rp')$, $\frac{\partial}{\partial z}[r\rho\langle w''^2\rangle_c]$ and $\frac{\partial}{\partial z}[r\rho\langle w''\varphi''\rangle_c]$ can be neglected. Since in this paper we only present a theoretical framework, we consider this approximation only for the simplicity of the exposure. However, one may retain these terms when building a specific parameterization scheme, but then additional closures are required. One may also consider that the contribution of these terms can be implicitly considered in the tuning parameters C_{mix} and $C_{mix,\varphi}$ (see Section 4.3.2), but this procedure requires further testing and validation.

Finally, an equation for the conservation of the kinetic energy may be obtained from the momentum equation. Rearranging the momentum Equation 94 as:

$$\frac{\partial}{\partial t}(r\rho w') + w'\frac{\partial}{\partial z}(r\rho w') + u_r'\frac{\partial}{\partial r}(r\rho w') = r\rho B' - \frac{\partial}{\partial r}(r\rho\tau_w), \tag{96}$$

and multiplying with w', after some manipulations, and using the continuity Equation 93, we obtain:

$$\frac{\partial}{\partial t}\left(\frac{1}{2}r\rho w'^2\right) + \frac{\partial}{\partial z}\left(\frac{1}{2}r\rho w'^3\right) + \frac{\partial}{\partial r}\left(\frac{1}{2}r\rho u_r' w'^2\right) = r\rho w' B' - w'\frac{\partial}{\partial r}(r\rho\tau_w). \tag{97}$$

B | APPROXIMATE ANALYTICAL SOLUTIONS

Considering that between the vertical grids of the parent numerical model, the slope of the plume radius could be considered linear with an accurate approximation, we may write:

$$R(z) = R_k + \alpha_k(z - z_k), \tag{98}$$

where R_k and α_k are the plume radius and the slope of the plume radius at the level z_k of the parent numerical model, as is schematically presented in Figure 6. We also consider that the density can be written as $\rho = \rho_k + \gamma_k(z - z_k)$ between the levels z_k and z_{k+1}, where ρ_k is the density at the k level and γ_k is the vertical gradient of the density at the level k.

From Equation 40 we can obtain an approximate value for α_k, as:

$$\alpha_k \approx \eta_5\frac{B_{c,k}' R_k}{w_{c,k}'^2} + \eta_6 - \frac{R_k\gamma_k}{2\rho_k}, \tag{99}$$

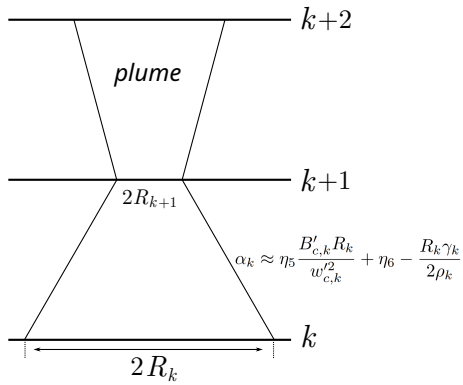

FIGURE 6 A schematic draw of a convective plume between the vertical grids of the parent numerical model.

where $B'_{c,k}$ and $w'_{c,k}$ are the centerline buoyancy and vertical velocity at the level z_k, respectively, and where we used that $d(\ln\rho)/dz \approx \gamma_k/\rho_k$. Therefore, the plume radius is updated at every vertical level k following Equations 98 and 99.

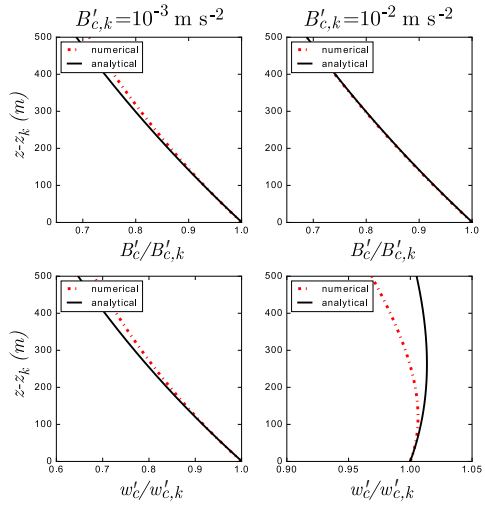

FIGURE 7 Graphical representation of the analytical solutions (black solid line) for the buoyancy (top row) and updraft velocity (bottom row) normalized by their initial values for a non−stratified environment ($N^2 = 0$), and the corresponding numerical solutions (red dash-dotted line). The initial vertical velocity and initial radius are set to 3 m s^{-1} and 200 m for all cases. The initial buoyancy is set to 10^{-3} m s^{-2} in the left column and 10^{-2} m s^{-2} in the right column. For simplicity, top−hat profiles are assumed and the Boussinesq approximation is used. The turbulent fluxes have been set as following: $f_\tau(1) = 0.2$ and $j_B(1) = 0.15$.

If we consider that between the vertical grids k and $k+1$, the plume radius is quasi−constant, then we can consider the approximation:

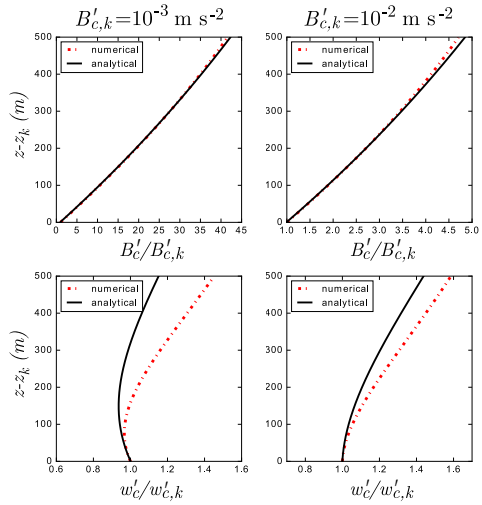

FIGURE 8 As in Figure 7 but for an unstable environment ($N^2 = -10^{-4}$ s^{-2}).

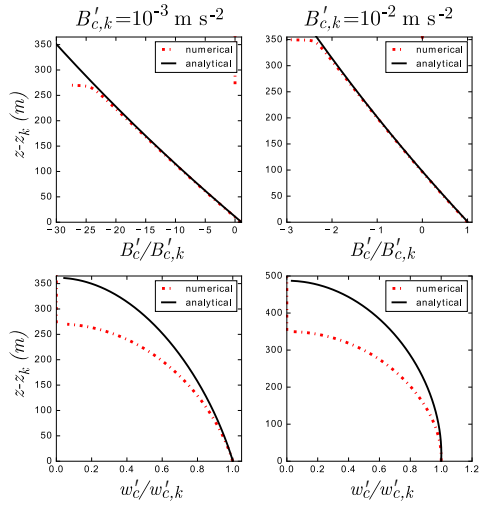

FIGURE 9 As in Figure 7 but for an stable environment ($N^2 = 10^{-4}$ s^{-2}).

$$\frac{1}{R}\frac{dR}{dz} \approx \frac{\alpha_k}{R_k}. \tag{100}$$

and thus, the system of Equations 36, 37 becomes:

$$\frac{dw_c'^2}{dz} = \frac{a_2}{a_1} B'_c - \Lambda_1 w_c'^2, \tag{101}$$

$$\frac{d\varphi_c'}{dz} = \frac{1}{a_6 w_c' R_k^2} J_c^{\varphi} - \frac{a_7}{a_6}\frac{\partial \overline{\varphi}}{\partial z} - \Lambda_2 \varphi_c', \tag{102}$$

where the terms Λ_1 and Λ_2 are given by:

$$\Lambda_1 = \frac{\eta_1 + 2\alpha_k}{R_k} + \frac{\gamma_k}{\rho_k}, \tag{103}$$

$$\Lambda_2 = \frac{\eta_2 + \eta_3 \alpha_k}{R_k} + \eta_4 \frac{\gamma_k}{\rho_k}. \tag{104}$$

Equations 101 and 102 have the following solutions:

$$w_c'^2(z) = \left[\frac{a_2}{a_1}\int_{z_k}^{z} B_c'(z') e^{\Lambda_1 (z'-z_k)} dz' + w_{c,k}'^2\right] e^{-\Lambda_1 (z-z_k)}, \tag{105}$$

$$\varphi_c'(z) = \left[\int_{z_k}^{z}\left[\frac{1}{a_6 w_c' R_k^2} J_c^{\varphi} - \frac{a_7}{a_6}\frac{\partial \overline{\varphi}}{\partial z}\right] e^{\Lambda_2 (z'-z_k)} dz' + \varphi_{c,k}'\right] e^{-\Lambda_2 (z-z_k)}. \tag{106}$$

Considering that J_c^{φ} and $\partial\overline{\varphi}/\partial z$ remain approximately constant between z_k and z_{k+1}, and that $1/w_c' \approx 1/w_{c,k}'$, we can obtain an approximate form for φ_c', as:

$$\varphi_c'(z) = \left[\left[\frac{1}{a_6 w_{c,k}' R_k^2} J_{c,k}^{\varphi} - \frac{a_7}{a_6}\left.\frac{\partial \overline{\varphi}}{\partial z}\right|_{z=z_k}\right]\frac{1}{\Lambda_2}\left(e^{\Lambda_2 (z-z_k)} - 1\right) + \varphi_{c,k}'\right] e^{-\Lambda_2 (z-z_k)}. \tag{107}$$

where $J_{c,k}^{\varphi}$ is the integral convective source term of the variable φ at the level z_k. Thus, for a constant N^2, for the updraft velocity we obtain:

$$\begin{aligned} w_c'(z) \quad = \quad & \left[\frac{a_2}{a_1}\left(B_{c,k}' + \frac{N^2}{\Lambda_2}\right)\frac{1}{\Lambda_1 - \Lambda_2}\left[e^{(\Lambda_1 - \Lambda_2)(z-z_k)} - 1\right] - \frac{a_2}{a_1}\frac{N^2}{\Lambda_1 \Lambda_2}\left[e^{\Lambda_1 (z-z_k)} - 1\right] + w_{c,k}'^2\right]^{1/2} \\ & e^{-\frac{1}{2}\Lambda_1 (z-z_k)}. \end{aligned} \tag{108}$$

In Figure 7 the analytical solutions for buoyancy (Equation 107) and updraft velocity (Equation 108) are compared with the numerical solutions for the neutral case with top–hat profiles. The numerical solutions are obtained by solving numerically the system of Equations (36), (39) and (40) using the Euler method at a resolution of 500 grid points and a vertical domain of 500 m. In both numerical and analytical representations the density vertical gradient has been neglected ($\delta_k = 0$). In Figures 8 and Figures 9 the same comparison is made for unstable and stable conditions,

respectively. As one may see, the analytical solutions show a very good agreement with the numerical ones, which are taken as reference.

Acknowledgements

The author acknowledges the financial support from the Romanian Ministry of Education consisting in a doctoral scholarship received through the Doctoral School of Physics of the University of Bucharest and from the Romanian Ministry of Research, Innovation and Digitisation through Project PN 23 21 01 01. The author thanks Robert Plant and two anonymous reviewers for valuable feedback and comments.

Conflict of interest

The author declare no conflict of interest.

ORCID

Cristian V. Vraciu https://orcid.org/0000-0003-1939-3230

references

Albright, A. L., Bony, S., Stevens, B. and Vogel, R. (2022) Observed subcloud-layer moisture and heat budgets in the trades. *Journal of the Atmospheric Sciences*, **79**, 2363–2385.

Angevine, W. M., Jiang, H. and Mauritsen, T. (2010) Performance of an eddy–diffusivity mass–flux scheme for shallow cumulus boundary layers. *Monthly Weather Review*, **138**, 2895–2912.

Arakawa, A. and Schubert, W. H. (1974) Interaction of a cumulus cloud ensemble with the large-scale environment, part i. *Journal of Atmospheric Sciences*, **31**, 674–701.

Arakawa, A. and Wu, C.-M. (2013) A unified representation of deep moist convection in numerical modeling of the atmosphere. part i. *Journal of the Atmospheric Sciences*, **70**, 1977–1992.

— (2015) Reply to "comments on 'a unified representation of deep moist convection in numerical modeling of the atmosphere. part i'". *Journal of the Atmospheric Sciences*, **72**, 2566–2567.

Bechtold, P., Bazile, E., Guichard, F., Mascart, P. and Richard, E. (2001) A mass-flux convection scheme for regional and global models. *Quarterly Journal of the Royal Meteorological Society*, **127**, 869–886.

Bejan, A. (2013) *Convection heat transfer*. John wiley & sons.

Bengtsson, L., Gerard, L., Han, J., Gehne, M., Li, W. and Dias, J. (2022) A prognostic-stochastic and scale-adaptive cumulus convection closure for improved tropical variability and convective gray-zone representation in noaa's unified forecast system (ufs). *Monthly Weather Review*, **150**, 3211–3227.

Betts, A. K. (1976) Modeling subcloud layer structure and interaction with a shallow cumulus layer. *Journal of the Atmospheric Sciences*, **33**, 2363–2382.

Bretherton, C. S., McCaa, J. R. and Grenier, H. (2004) A new parameterization for shallow cumulus convection and its application to marine subtropical cloud-topped boundary layers. part i: Description and 1d results. *Monthly Weather Review*, **132**, 864–882.

Bryan, G. H., Wyngaard, J. C. and Fritsch, J. M. (2003) Resolution requirements for the simulation of deep moist convection. *Monthly Weather Review*, **131**, 2394–2416.

Chu, W. and Lin, Y. (2023) Description and evaluation of a new deep convective cloud model considering in-cloud inhomogeneity. *Journal of Advances in Modeling Earth Systems*, **15**, e2022MS003119.

Cohen, Y., Lopez-Gomez, I., Jaruga, A., He, J., Kaul, C. M. and Schneider, T. (2020) Unified entrainment and detrainment closures for extended eddy-diffusivity mass-flux schemes. *Journal of Advances in Modeling Earth Systems*, **12**, e2020MS002162.

D'Andrea, F., Gentine, P., Betts, A. K. and Lintner, B. R. (2014) Triggering deep convection with a probabilistic plume model. *Journal of the Atmospheric Sciences*, **71**, 3881–3901.

Dawe, J. T. and Austin, P. H. (2011) Interpolation of les cloud surfaces for use in direct calculations of entrainment and detrainment. *Monthly Weather Review*, **139**, 444–456.

Denby, L., Böing, S. J., Parker, D. J., Ross, A. N. and Tobias, S. M. (2022) Characterising the shape, size, and orientation of cloud-feeding coherent boundary-layer structures. *Quarterly Journal of the Royal Meteorological Society*, **148**, 499–519.

Deremble, B. (2016) Convective plumes in rotating systems. *Journal of Fluid Mechanics*, **799**, 27–55.

Ezzamel, A., Salizzoni, P. and Hunt, G. R. (2015) Dynamical variability of axisymmetric buoyant plumes. *Journal of Fluid Mechanics*, **765**, 576–611.

Fan, J. et al. (2015) Improving representation of convective transport for scale-aware parameterization: 1. convection and cloud properties simulated with spectral bin and bulk microphysics. *Journal of Geophysical Research: Atmospheres*, **120**, 3485–3509.

Gerard, L. (2015) Bulk mass-flux perturbation formulation for a unified approach of deep convection at high resolution. *Monthly Weather Review*, **143**, 4038–4063.

Gerard, L. and Geleyn, J.-F. (2005) Evolution of a subgrid deep convection parametrization in a limited-area model with increasing resolution. *Quarterly Journal of the Royal Meteorological Society*, **131**, 2293–2312.

Gregory, D. (2001) Estimation of entrainment rate in simple models of convective clouds. *Quarterly Journal of the Royal Meteorological Society*, **127**, 53–72.

Grell, G. A. and Freitas, S. R. (2014) A scale and aerosol aware stochastic convective parameterization for weather and air quality modeling. *Atmospheric Chemistry and Physics*, **14**, 5233–5250.

Griewank, P. J., Heus, T., Lareau, N. P. and Neggers, R. A. (2020) Size dependence in chord characteristics from simulated and observed continental shallow cumulus. *Atmospheric Chemistry and Physics*, **20**, 10211–10230.

Gu, J.-F., Plant, R. S., Holloway, C. E. and Jones, T. R. (2021) Composited structure of non-precipitating shallow cumulus clouds. *Quarterly Journal of the Royal Meteorological Society*, **147**, 2818–2833.

Hagos, S., Chen, J., Barber, K., Sakaguchi, K., Plant, R. S., Feng, Z. and Xiao, H. (2022) A machine-learning-assisted stochastic cloud population model as a parameterization of cumulus convection. *Journal of Advances in Modeling Earth Systems*, **14**, e2021MS002808.

Hagos, S., Feng, Z., Plant, R. S., Houze Jr, R. A. and Xiao, H. (2018) A stochastic framework for modeling the population dynamics of convective clouds. *Journal of Advances in Modeling Earth Systems*, **10**, 448–465.

Han, J. and Bretherton, C. S. (2019) Tke–based moist eddy–diffusivity mass–flux (edmf) parameterization for vertical turbulent mixing. *Weather and Forecasting*, **34**, 869–886.

Hohenegger, C. and Bretherton, C. S. (2011) Simulating deep convection with a shallow convection scheme. *Atmospheric Chemistry and Physics*, **11**, 10389–10406.

Holloway, C. E. et al. (2014) Understanding and representing atmospheric convection across scales: Recommendations from the meeting held at dartington hall, devon, uk, 28–30 january 2013. *Atmospheric Science Letters*, **15**, 348–353.

Hourdin, F., Couvreux, F. and Menut, L. (2002) Parameterization of the dry convective boundary layer based on a mass flux representation of thermals. *Journal of the Atmospheric Sciences*, **59**, 1105–1123.

Houze, R. A. (2014) *Cloud dynamics*. Academic press.

Jeevanjee, N. (2017) Vertical velocity in the gray zone. *Journal of Advances in Modeling Earth Systems*, **9**, 2304–2316.

Kain, J. S. and Fritsch, J. M. (1990) A one-dimensional entraining/detraining plume model and its application in convective parameterization. *Journal of Atmospheric Sciences*, **47**, 2784–2802.

Kaminski, E., Tait, S. and Carazzo, G. (2005) Turbulent entrainment in jets with arbitrary buoyancy. *Journal of Fluid Mechanics*, **526**, 361–376.

Kewalramani, G., Pant, C. S. and Bhattacharya, A. (2022) Energy consistent gaussian integral model for jet with off-source heating. *Physical Review Fluids*, **7**, 013801.

Khairoutdinov, M. F., Krueger, S. K., Moeng, C.-H., Bogenschutz, P. A. and Randall, D. A. (2009) Large-eddy simulation of maritime deep tropical convection. *Journal of Advances in Modeling Earth Systems*, **1**.

Kim, D. and Kang, I.-S. (2012) A bulk mass flux convection scheme for climate model: Description and moisture sensitivity. *Climate dynamics*, **38**, 411–429.

Klocke, D., Pincus, R. and Quaas, J. (2011) On constraining estimates of climate sensitivity with present-day observations through model weighting. *Journal of Climate*, **24**, 6092–6099.

Kriegmair, R., Ruckstuhl, Y., Rasp, S. and Craig, G. (2022) Using neural networks to improve simulations in the gray zone. *Nonlinear Processes in Geophysics*, **29**, 171–181.

Kwon, Y. C. and Hong, S.-Y. (2017) A mass-flux cumulus parameterization scheme across gray-zone resolutions. *Monthly Weather Review*, **145**, 583–598.

Langguth, M., Kuell, V. and Bott, A. (2020) Implementing the hybrid mass flux convection scheme (hymacs) in icon–first idealized tests and adaptions to the dynamical core for local mass sources. *Quarterly Journal of the Royal Meteorological Society*, **146**, 2689–2716.

Lebo, Z. and Morrison, H. (2015) Effects of horizontal and vertical grid spacing on mixing in simulated squall lines and implications for convective strength and structure. *Monthly Weather Review*, **143**, 4355–4375.

Lopez-Gomez, I., Christopoulos, C., Langeland Ervik, H. L., Dunbar, O. R., Cohen, Y. and Schneider, T. (2022) Training physics-based machine-learning parameterizations with gradient-free ensemble kalman methods. *Journal of Advances in Modeling Earth Systems*, **14**, e2022MS003105.

Malardel, S. and Bechtold, P. (2019) The coupling of deep convection with the resolved flow via the divergence of mass flux in the ifs. *Quarterly Journal of the Royal Meteorological Society*, **145**, 1832–1845.

Mallaun, C., Giez, A., Mayr, G. J. and Rotach, M. W. (2019) Subsiding shells and the distribution of up-and downdraughts in warm cumulus clouds over land. *Atmospheric Chemistry and Physics*, **19**, 9769–9786.

Masson-Delmotte, V., Zhai, P., Pirani, A., Connors, S. L., Péan, C., Berger, S., Caud, N., Chen, Y., Goldfarb, L., Gomis, M. et al. (eds.) (2021) *Climate change 2021: The physical science basis. Contribution of working group I to the sixth assessment report of the intergovernmental panel on climate change*. Cambridge University Press.

Milton-McGurk, L., Williamson, N. and Armfield, S. (2023) Predicting radial profiles for jets with arbitrary buoyancy. *Journal of Fluid Mechanics*, **956**, A9.

Morton, B. R., Taylor, G. I. and Turner, J. S. (1956) Turbulent gravitational convection from maintained and instantaneous sources. *Proceedings of the Royal Society A*, **234**, 1–23.

Murphy, J. M., Sexton, D. M., Barnett, D. N., Jones, G. S., Webb, M. J., Collins, M. and Stainforth, D. A. (2004) Quantification of modelling uncertainties in a large ensemble of climate change simulations. *Nature*, **430**, 768–772.

Nair, V., Heus, T. and Van Reeuwijk, M. (2020) Dynamics of subsiding shells in actively growing clouds with vertical updrafts. *Journal of the Atmospheric Sciences*, **77**, 1353–1369.

Neggers, R., Siebesma, A. and Jonker, H. (2002) A multiparcel model for shallow cumulus convection. *Journal of the Atmospheric Sciences*, **59**, 1655–1668.

Neggers, R., Stevens, B. and Neelin, J. D. (2006) A simple equilibrium model for shallow-cumulus-topped mixed layers. *Theoretical and Computational Fluid Dynamics*, **20**, 305–322.

O'Gorman, P. A. and Dwyer, J. G. (2018) Using machine learning to parameterize moist convection: Potential for modeling of climate, climate change, and extreme events. *Journal of Advances in Modeling Earth Systems*, **10**, 2548–2563.

Pan, D.-M. and Randall, D. D. (1998) A cumulus parameterization with a prognostic closure. *Quarterly Journal of the Royal Meteorological Society*, **124**, 949–981.

Park, S. (2014) A unified convection scheme (unicon). part i: Formulation. *Journal of the Atmospheric Sciences*, **71**, 3902–3930.

Pergaud, J., Masson, V., Malardel, S. and Couvreux, F. (2009) A parameterization of dry thermals and shallow cumuli for mesoscale numerical weather prediction. *Boundary–Layer Meteorology*, **132**, 83–106.

Peters, J. M., Morrison, H., Varble, A. C., Hannah, W. M. and Giangrande, S. E. (2020) Thermal chains and entrainment in cumulus updrafts. part ii: Analysis of idealized simulations. *Journal of the Atmospheric Sciences*, **77**, 3661–3681.

Peters, J. M., Morrison, H., Zhang, G. J. and Powell, S. (2021) Improving the physical basis for updraft dynamics in deep convection parameterizations. *Journal of Advances in Modeling Earth Systems*, **13**, e2020MS002282.

Pinsky, M., Eytan, E., Koren, I., Altaratz, O. and Khain, A. (2021) Convective and turbulent motions in nonprecipitating cu. part i: Method of separation of convective and turbulent motions. *Journal of the Atmospheric Sciences*, **78**, 2307–2321.

Pinsky, M. and Khain, A. (2023) Convective and turbulent motions in nonprecipitating cu. part iii: Characteristics of turbulence motions. *Journal of the Atmospheric Sciences*, **80**, 457–471.

Plant, R. and Craig, G. C. (2008) A stochastic parameterization for deep convection based on equilibrium statistics. *Journal of the Atmospheric Sciences*, **65**, 87–105.

Plant, R. S. (2010) A review of the theoretical basis for bulk mass flux convective parameterization. *Atmospheric Chemistry and Physics*, **10**, 3529–3544.

Plant, R. S. and Yano, J.-I. (eds.) (2016) *Parameterization of atmospheric convection*. Imperial College Press.

Priestley, C. and Ball, F. (1955) Continuous convection from an isolated source of heat. *Quarterly Journal of the Royal Meteorological Society*, **81**, 144–157.

van Reeuwijk, M. and Craske, J. (2015) Energy-consistent entrainment relations for jets and plumes. *Journal of Fluid Mechanics*, **782**, 333–355.

van Reeuwijk, M., Salizzoni, P., Hunt, G. R. and Craske, J. (2016) Turbulent transport and entrainment in jets and plumes: a dns study. *Physical Review Fluids*, **1**, 074301.

Rio, C. and Hourdin, F. (2008) A thermal plume model for the convective boundary layer: Representation of cumulus clouds. *Journal of the Atmospheric Sciences*, **65**, 407–425.

Rio, C., Hourdin, F., Grandpeix, J.-Y. and Lafore, J.-P. (2009) Shifting the diurnal cycle of parameterized deep convection over land. *Geophysical Research Letters*, **36**.

Romps, D. M. (2010) A direct measure of entrainment. *Journal of the Atmospheric Sciences*, **67**, 1908–1927.

Romps, D. M. and Charn, A. B. (2015) Sticky thermals: Evidence for a dominant balance between buoyancy and drag in cloud updrafts. *Journal of the Atmospheric Sciences*, **72**, 2890–2901.

de Roode, S. R., Duynkerke, P. G. and Siebesma, A. P. (2000) Analogies between mass-flux and reynolds-averaged equations. *Journal of the Atmospheric Sciences*, **57**, 1585–1598.

de Roode, S. R., Siebesma, A. P., Jonker, H. J. J. and de Voogd, Y. (2012) Parameterization of the vertical velocity equation for shallow cumulus clouds. *Monthly Weather Review*, **140**, 2424–2436.

de Rooy, W. C. et al. (2013) Entrainment and detrainment in cumulus convection: An overview. *Quarterly Journal of the Royal Meteorological Society*, **139**, 1–19.

Sakradzija, M. and Klocke, D. (2018) Physically constrained stochastic shallow convection in realistic kilometer-scale simulations. *Journal of Advances in Modeling Earth Systems*, **10**, 2755–2776.

Sakradzija, M., Seifert, A. and Dipankar, A. (2016) A stochastic scale-aware parameterization of shallow cumulus convection across the convective gray zone. *Journal of Advances in Modeling Earth Systems*, **8**, 786–812.

von Salzen, K. and McFarlane, N. A. (2002) Parameterization of the bulk effects of lateral and cloud-top entrainment in transient shallow cumulus clouds. *Journal of the Atmospheric Sciences*, **59**, 1405–1430.

Savre, J. (2021) Formation and maintenance of subsiding shells around non-precipitating and precipitating cumulus clouds. *Quarterly Journal of the Royal Meteorological Society*, **147**, 728–745.

Savre, J. and Craig, G. (2023) The sensitivity of convective cloud ensemble statistics to horizontal grid spacing in idealized rce simulations. *Journal of the Atmospheric Sciences*, **80**, 1267–1284.

Savre, J. and Herzog, M. (2019) A general description of entrainment in buoyant cloudy plumes including the effects of mixing-induced evaporation. *Journal of the Atmospheric Sciences*, **76**, 479–496.

Sherwood, S. et al. (2020) An assessment of earth's climate sensitivity using multiple lines of evidence. *Reviews of Geophysics*, **58**, e2019RG000678.

Shin, J. and Baik, J.-J. (2022) Parameterization of stochastically entraining convection using machine learning technique. *Journal of Advances in Modeling Earth Systems*, **14**, e2021MS002817.

Shin, J. and Park, S. (2020) A stochastic unified convection scheme (unicon). part i: Formulation and single-column simulation for shallow convection. *Journal of the Atmospheric Sciences*, **77**, 583–610.

Siebesma, A. P., Soares, P. M. and Teixeira, J. (2007) A combined eddy–diffusivity mass-flux approach for the convective boundary layer. *Journal of the Atmospheric Sciences*, **64**, 1230–1248.

Siebesma, A. P. and Teixeira, J. (2000) An advection–diffusion scheme for the convective boundary layer: Description and 1d results. In *Preprints, 14th Symp. on Boundary Layers and Turbulence, Aspen, CO, Amer. Meteor. Soc*, 133–136.

Smalley, M., Suselj, K., Lebsock, M. and Witte, M. (2022) Coupling warm rain with an eddy diffusivity/mass flux parameterization: 2. sensitivities and comparison to observations. *Journal of Advances in Modeling Earth Systems*, **14**, e2021MS002729.

Soares, P., Miranda, P., Siebesma, A. and Teixeira, J. (2004) An eddy–diffusivity/mass–flux parametrization for dry and shallow cumulus convection. *Quarterly Journal of the Royal Meteorological Society*, **130**, 3365–3383.

Suselj, K., Kurowski, M. J. and Teixeira, J. (2019) A unified eddy-diffusivity/mass-flux approach for modeling atmospheric convection. *Journal of the Atmospheric Sciences*, **76**, 2505–2537.

Suselj, K., Smalley, M., Lebsock, M. D., Kurowski, M. J., Witte, M. K. and Teixeira, J. (2022) Coupling warm rain with an eddy diffusivity/mass flux parameterization: 1. model description and validation. *Journal of Advances in Modeling Earth Systems*, **14**, e2021MS002736.

Sušelj, K., Teixeira, J. and Matheou, G. (2012) Eddy diffusivity/mass flux and shallow cumulus boundary layer: An updraft pdf multiple mass flux scheme. *Journal of the Atmospheric Sciences*, **69**, 1513–1533.

Tan, Z., Kaul, C. M., Pressel, K. G., Cohen, Y., Schneider, T. and Teixeira, J. (2018) An extended eddy-diffusivity mass-flux scheme for unified representation of subgrid-scale turbulence and convection. *Journal of Advances in Modeling Earth Systems*, **10**, 770–800.

Thuburn, J., Weller, H., Vallis, G. K., Beare, R. J. and Whitall, M. (2018) A framework for convection and boundary layer parameterization derived from conditional filtering. *Journal of the Atmospheric Sciences*, **75**, 965–981.

Tiedtke, M. (1989) A comprehensive mass flux scheme for cumulus parameterization in large-scale models. *Monthly Weather Review*, **117**, 1779–1800.

Turner, J. (1986) Turbulent entrainment: the development of the entrainment assumption, and its application to geophysical flows. *Journal of Fluid Mechanics*, **173**, 431–471.

Vraciu, C. V. (2022) On the energy–consistent plume model in the convective boundary layer. *Dynamics of Atmospheres and Oceans*, **100**, 101330.

Wang, H. and Law, A. W.-k. (2002) Second-order integral model for a round turbulent buoyant jet. *Journal of Fluid Mechanics*, **459**, 397–428.

Wang, W. (2022) Forecasting convection with a 'scale-aware' tiedtke cumulus parameterization scheme at kilometer scales. *Weather and Forecasting*, **37**, 1491–1507.

Witte, M. K. et al. (2022) Augmenting the double-gaussian representation of atmospheric turbulence and convection via a coupled stochastic multi-plume mass flux scheme. *Monthly Weather Review*, **150**, 2339–2355.

Yano, J.-I. (2012) Mass-flux subgrid-scale parameterization in analogy with multi-component flows: a formulation towards scale independence. *Geoscientific Model Development*, **5**, 1425–1440.

— (2014a) Basic convective element: bubble or plume? a historical review. *Atmospheric Chemistry and Physics*, **14**, 7019–7030.

— (2014b) Formulation structure of the mass-flux convection parameterization. *Dynamics of Atmospheres and Oceans*, **67**, 1–28.

— (2016) Subgrid-scale physical parameterization in atmospheric modeling: How can we make it consistent? *Journal of Physics A: Mathematical and Theoretical*, **49**, 284001.

— (2023) Plume. In *Geophysical Convection Dynamics* (ed. J.-I. Yano), vol. 5 of *Developments in Weather and Climate Science*, 251–267. Elsevier.

Yano, J.-I., Bénard, P., Couvreux, F. and Lahellec, A. (2010) Nam–sca: A nonhydrostatic anelastic model with segmentally constant approximations. *Monthly weather review*, **138**, 1957–1974.

Yano, J.-I., Bengtsson, L., Geleyn, J.-F. and Brozkova, R. (2016) Towards a unified and self-consistent parameterization framework. In *Parameterization of Atmospheric Convection*, 423–435. Imperial College Press.

Yano, J.-I., Bister, M., Fuchs, Ž., Gerard, L., Phillips, V., Barkidija, S. and Piriou, J.-M. (2013) Phenomenology of convection-parameterization closure. *Atmospheric Chemistry and Physics*, **13**, 4111–4131.

Yano, J.-I. et al. (2018) Scientific challenges of convective-scale numerical weather prediction. *Bulletin of the American Meteorological Society*, **99**, 699–710.

Yin, J. and Porporato, A. (2017) Diurnal cloud cycle biases in climate models. *Nature communications*, **8**, 2269.

Yuval, J. and O'Gorman, P. A. (2020) Stable machine-learning parameterization of subgrid processes for climate modeling at a range of resolutions. *Nature communications*, **11**, 3295.

Zheng, Y., Alapaty, K., Herwehe, J. A., Del Genio, A. D. and Niyogi, D. (2016) Improving high-resolution weather forecasts using the weather research and forecasting (wrf) model with an updated kain–fritsch scheme. *Monthly Weather Review*, **144**, 833–860.